






Orientia tsutsugamushi Nucleomodulin Ank13 Exploits the RaDAR Nuclear Import Pathway To Modulate Host Cell Transcription

Haley E. Adcox,^a Amanda L. Hatke,^a Shelby E. Andersen,^b Sarika Gupta,^a Nathan B. Otto,^a  Mary M. Weber,^b  Richard T. Marconi,^a  Jason A. Carlyon^a

^aDepartment of Microbiology and Immunology, Virginia Commonwealth University Medical Center, School of Medicine, Richmond, Virginia, USA

^bDepartment of Microbiology and Immunology, University of Iowa Health Care, Carver College of Medicine, Iowa City, Iowa, USA

ABSTRACT *Orientia tsutsugamushi* is the etiologic agent of scrub typhus, the deadliest of all diseases caused by obligate intracellular bacteria. Nucleomodulins, bacterial effectors that dysregulate eukaryotic transcription, are being increasingly recognized as key virulence factors. How they translocate into the nucleus and their functionally essential domains are poorly defined. We demonstrate that Ank13, an *O. tsutsugamushi* effector conserved among clinical isolates and expressed during infection, localizes to the nucleus in an importin β 1-independent manner. Rather, Ank13 nucleotropism requires an isoleucine at the thirteenth position of its fourth ankyrin repeat, consistent with utilization of eukaryotic RaDAR (RanGDP-ankyrin repeats) nuclear import. RNA-seq analyses of cells expressing green fluorescent protein (GFP)-tagged Ank13, nucleotropism-deficient Ank13_{1127R} or Ank13 Δ F-box, which lacks the F-box domain essential for interacting with SCF ubiquitin ligase, revealed Ank13 to be a nucleomodulin that predominantly downregulates transcription of more than 2,000 genes. Its ability to do so involves its nucleotropism and F-box in synergistic and mutually exclusive manners. Ank13 also acts in the cytoplasm to dysregulate smaller cohorts of genes. The effector's toxicity in yeast heavily depends on its F-box and less so on its nucleotropism. Genes negatively regulated by Ank13 include those involved in the inflammatory response, transcriptional control, and epigenetics. Importantly, the majority of genes that GFP-Ank13 most strongly downregulates are quiescent or repressed in *O. tsutsugamushi*-infected cells when Ank13 expression is strongest. Ank13 is the first nucleomodulin identified to coopt RaDAR and a multifaceted effector that functions in the nucleus and cytoplasm via F-box-dependent and -independent mechanisms to globally reprogram host cell transcription.

IMPORTANCE Nucleomodulins are recently defined effectors used by diverse intracellular bacteria to manipulate eukaryotic gene expression and convert host cells into hospitable niches. How nucleomodulins enter the nucleus, their functional domains, and the genes that they modulate are incompletely characterized. *Orientia tsutsugamushi* is an intracellular bacterial pathogen that causes scrub typhus, which can be fatal. *O. tsutsugamushi* Ank13 is the first example of a microbial protein that coopts eukaryotic RaDAR (RanGDP-ankyrin repeats) nuclear import. It dysregulates expression of a multitude of host genes with those involved in transcriptional control and the inflammatory response being among the most prominent. Ank13 does so via mechanisms that are dependent and independent of both its nucleotropism and eukaryotic-like F-box domain that interfaces with ubiquitin ligase machinery. Nearly all the genes most strongly downregulated by ectopically expressed Ank13 are repressed in *O. tsutsugamushi*-infected cells, implicating its importance for intracellular colonization and scrub typhus molecular pathogenesis.

Citation Adcox HE, Hatke AL, Andersen SE, Gupta S, Otto NB, Weber MM, Marconi RT, Carlyon JA. 2021. *Orientia tsutsugamushi* nucleomodulin Ank13 exploits the RaDAR nuclear import pathway to modulate host cell transcription. *mBio* 12:e01816-21. <https://doi.org/10.1128/mBio.01816-21>.

Editor Craig R. Roy, Yale University School of Medicine

Copyright © 2021 Adcox et al. This is an open-access article distributed under the terms of the [Creative Commons Attribution 4.0 International license](https://creativecommons.org/licenses/by/4.0/).

Address correspondence to Jason A. Carlyon, jason.carlyon@vcuhealth.org.

This article is a direct contribution from Jason A. Carlyon, a Fellow of the American Academy of Microbiology, who arranged for and secured reviews by Roman Ganta, Kansas State University, and Sean Riley, University of Maryland.

Received 19 June 2021

Accepted 1 July 2021

Published 3 August 2021

KEYWORDS *Orientia tsutsugamushi*, *Rickettsia*, ankyrin repeat, bacterial effector, intracellular bacterium, nucleomodulin

Nucleomodulins are an emerging family of bacterial effectors that traffic into the nucleus to selectively control gene expression and thereby regulate eukaryotic cellular processes. Nearly all known nucleomodulins are deployed by intracellular bacteria (1, 2). Despite their importance as intracellular microbial virulence factors, how they traffic into the nucleus, their functionally essential domains and residues, and the genes that they dysregulate are poorly defined. Hence, characterizing nucleomodulins stands to reveal novel mechanisms by which intracellular bacteria remodel their host cells into permissive niches.

Orientia tsutsugamushi is a mite-transmitted obligate intracellular bacterium and the leading cause of scrub typhus, a severe infection prevalent in the Asia-Pacific region, where approximately one million new cases occur annually (3, 4). Locally acquired cases in the Middle East and South America, along with numerous travel-acquired cases, signify the disease as a global health threat (4–8). Acute symptoms include fever, headache, rash, and lymphadenopathy. If antibiotic therapy is delayed, scrub typhus can progress to pneumonitis, respiratory distress, meningitis, systemic vascular collapse, shock, organ failure, and death (3, 4). *O. tsutsugamushi* primarily invades monocytes, macrophages, and dendritic cells at the mite feeding site and disseminates via the lymphatics to invade endothelial cells of multiple organs (9). Within host cells, the bacterium replicates in the cytosol. While a type 1 inflammatory response is critical for both clearing and mediating immunopathological damage associated with scrub typhus (10–15), *O. tsutsugamushi* counteracts it and other host defense pathways (16–23), which likely contributes to its ability to successfully colonize host cells. The responsible bacterial factors and their mechanisms of action are largely unknown.

The 30- to 33-residue ankyrin repeat (AR) is one of the most common protein-protein interaction motifs in nature and a ubiquitous structural motif across the tree of life (24, 25). Analysis of more than 1,900 bacterial species revealed that obligate intracellular bacteria have the highest percentage of AR-containing proteins (Anks) within their proteomes, reflective of their prominence as interfaces with eukaryotic processes (24). Approximately 2.4% of the *O. tsutsugamushi* Ikeda strain genome encodes Anks, a percentage rivaling that of eukaryotes (24, 26). Specific *O. tsutsugamushi* Anks have been linked to the pathogen's abilities to impair nuclear factor kappa-light-chain-enhancer of activated B cells (NF- κ B) nuclear import, inhibit the secretory pathway, and degrade elongation factor 1 α (16, 27, 28). *O. tsutsugamushi* Anks are type 1 secretion system effectors and are transcriptionally expressed during infection of mammalian cells (29). They share a two-dimensional architecture, having an N-terminal domain comprised of various numbers of tandemly arranged ARs (26, 29). Most also carry a C-terminal domain that mimics the eukaryotic F-box, which interacts with Skp1 (S-phase kinase-associated protein 1) of SCF E3 ubiquitin ligase complexes (26, 28, 30, 31). The SCF complex consists of Skp1, cullin-1 (Cul1), ring box (Rbx1), and an additional adaptor protein that carries an E-box (31). For *O. tsutsugamushi* and other microbial F-box-containing Anks, the prevailing model is that the AR domain binds a host cell target protein while the F-box binds Skp1 to nucleate the SCF complex, thereby orchestrating polyubiquitination of the AR-bound target and its degradation in the 26S proteasome (28, 30, 32–38).

Functions of most *O. tsutsugamushi* Anks remain to be determined. Our previous qualitative screen of the subcellular locations of the distinguishable 19 *O. tsutsugamushi* strain Ikeda Anks when ectopically expressed revealed that GFP- or Flag-tagged Ank13 (OTT_RS04140) was the only one to robustly accumulate in the nucleus whether the fusion tag was N or C terminal (29). Since this result is consistent with those observed for other pathogens' nucleomodulins (39, 40), we examined here whether Ank13 is a nucleomodulin. Our findings establish Ank13 as a *bona fide* nucleomodulin and the first example of an effector that exploits the eukaryotic RaDAR (RanGDP-

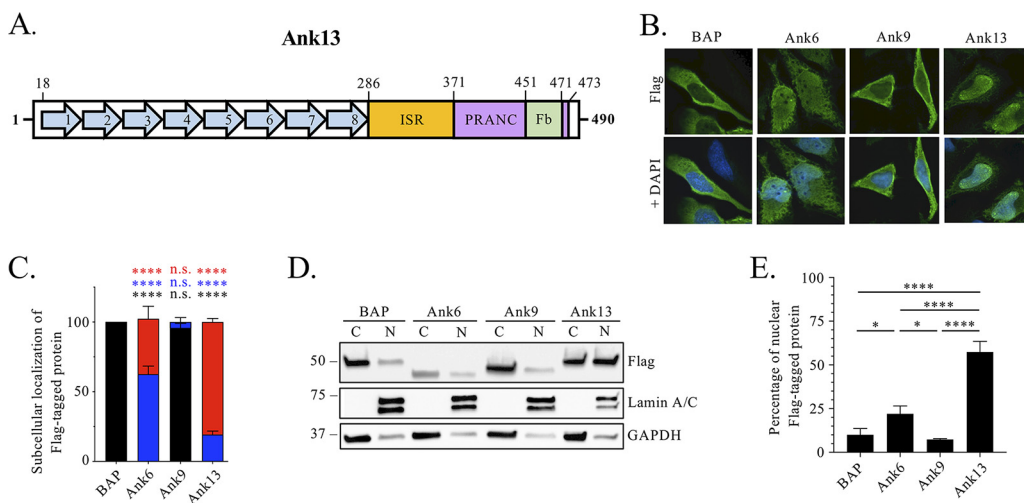


FIG 1 Ank13 is nucleotropic. (A) Schematic of Ank13 depicting its eight tandemly arranged ankyrin repeats (blue arrows), ISR (orange), and F-box (Fb; green). The Fb occurs as part of a larger encompassing PRANC domain (purple). Amino acids that constitute each domain are indicated. (B to E) Flag-Ank13 predominantly localizes to the nucleus. Transfected HeLa cells expressing Flag-tagged BAP, Ank6, Ank9, or Ank13 were examined by immunofluorescence microscopy (B and C) and Western blot analysis of nuclear [N] and cytoplasmic [C] fractions (D and E). (B) Representative images of fixed cells immunolabeled with Flag antibody and stained with DAPI. (C) One hundred cells were examined per condition in triplicate to quantify the means \pm the standard deviations (SD) for the percentages of cells exhibiting Flag immunosignal localization, which was scored as being exclusively cytoplasmic (black), throughout the cell (blue), or exclusively in the nucleus (red). Two-way ANOVA with Dunnett’s correction determined significance between subcellular locations of Flag-tagged proteins compared to Flag-BAP. The data are representative of three experiments with similar results. (D) Fractions were probed with lamin A/C and GAPDH antibodies to verify fraction purity and Flag antibody to determine localization of Flag-tagged protein. (E) The nuclear densitometric value was divided by the sum of nuclear and cytoplasmic densitometric values for Flag-tagged proteins in panel D. The quotient was multiplied by 100 to yield the percentage of Flag-tagged protein in the nucleus. Data presented are percentages (means \pm the SD) of Flag-tagged proteins exhibiting nuclear localization from three separate experiments. One-way ANOVA with Tukey’s *post hoc* test was used to test for significant difference in percentage of nuclear Flag-tagged protein among the conditions. Statistically significant values are indicated. *, $P < 0.05$; ****, $P < 0.0001$. n.s., not significant.

ankyrin repeats) nuclear import pathway. It downregulates cohorts of host genes, including those involved in transcriptional control, mRNA stability, epigenetic regulation, cell cycle control, and the inflammatory response. Its nucleomodulin ability and toxicity in yeast are dependent on both its nucleotropism and F-box. Many genes that ectopically expressed GFP-Ank13 downregulates are also repressed in *O. tsutsugamushi*-infected cells at a time point coincident with bacterial Ank13 expression. This study advances understanding of how *O. tsutsugamushi* transcriptionally regulates diverse host cellular processes, identifies a novel mechanism of nucleomodulin nuclear translocation, and underscores the contribution of the bacterial F-box as a eukaryotic transcriptional modulator.

RESULTS

Ank13 is conserved among *O. tsutsugamushi* isolates from scrub typhus patients.

Ank13 of *O. tsutsugamushi* strain Ikeda, a human isolate from Japan that causes severe scrub typhus (41), is 490 amino acids in length (26, 29). It consists of eight tandemly arranged ARs in its N-terminal half, an 86-amino-acid intervening sequence region (ISR) that is unique to Ank13, and a C-terminal F-box that occurs as part of a PRANC (pox proteins repeats of ankyrin - C terminal) domain (Fig. 1A). It is encoded by a single-copy gene (26, 29). Using the National Center for Biotechnology Information (NCBI) Nucleotide Basic Local Alignment Search Tool (BLASTN) (www.blast.ncbi.nlm.nih.gov) with Ikeda *ank13* as the query identified homologs in *O. tsutsugamushi* Kato strain (Japan), Karp strain isolates UT76 and UT176 (both from northeastern Thailand), and the Wuj/2014 isolate (China), each of which were recovered from patients and for which the complete genomes are in GenBank (42, 43). These homologs exhibited 89 to

92% nucleotide identity, 77 to 81% amino acid identity, and 85 to 87% amino acid similarity with Ikeda Ank13 (see Table S1 in the supplemental material). Primers targeting conserved nucleotides were used to amplify a segment corresponding to Ikeda *ank13* nucleotides 853 to 1260 from Karp isolates UT169, UT177, and UT559 (northeastern Thailand), Gilliam strain isolate FPW2016 (western Thailand), and isolates TM2532 (Central Laos), and SV445 (southern Laos) (43–45) (see Fig. S1A), for which genomic sequences are not available in GenBank. Sequencing and aligning the amplicons and their predicated amino acid sequences revealed 88 to 96% nucleotide identity, 79 to 90% amino acid identity, and 85 to 93% amino acid similarity with the corresponding region of Ikeda Ank13 (see Fig. S1B and C). Thus, Ank13 is conserved among phylogenetically and geographically diverse *O. tsutsugamushi* isolates.

Ectopically expressed Ank13 robustly localizes to the nucleus. HeLa cells are excellent models for studying *O. tsutsugamushi*-host cell interactions because the bacterium's infection cycle proceeds comparably in them as in other mammalian cell types and their amenability to transfection allows for correlation between phenotypes observed for infected cells and cells ectopically expressing oriental virulence factors (16, 19, 22, 27, 46–49). To quantify the propensity of Ank13 to localize to the nucleus, HeLa cells transfected to express Flag-Ank13 were examined by indirect immunofluorescence microscopy (Fig. 1B). Subcellular distribution of Flag immunosignal was scored as cytoplasmic, throughout the cell, or nuclear (Fig. 1C; see also Fig. S2). Flag-tagged Ank6, an *O. tsutsugamushi* effector that cycles in and out of the nucleus to impair NF- κ B (16), was a positive control for nuclear localization. Negative controls for nuclear localization were Flag-tagged *O. tsutsugamushi* Ank9, a Golgi- and ER-tropic effector, and bacterial alkaline phosphatase (BAP), both of which predominantly remain in the cytoplasm but exhibit low level nuclear accumulation when ectopically expressed (16, 27, 29). Flag-Ank13 and Flag-Ank6 exclusively localized to the nucleus in 81 and 40% of transfected cells, respectively, with neither exhibiting strict cytoplasmic distribution (Fig. 1C). Flag-BAP exclusively and Flag-Ank9 near exclusively remained in the cytoplasm. These observations were validated when nuclear and cytoplasmic fractions of HeLa cells expressing the same four proteins were subjected to Western blotting. Screening the fractions with antibodies against the Flag tag, lamin A/C (nuclear fraction loading control), and glyceraldehyde-3-phosphate dehydrogenase (GAPDH; cytoplasmic fraction loading control) confirmed that Flag-Ank13 pronouncedly traffics to the nucleus and does so with a significantly greater efficiency than Flag-Ank6 (Fig. 1D and E).

***O. tsutsugamushi* temporally upregulates *ank13* expression late during infection.** Following entry into host cells, the *O. tsutsugamushi* population exhibits minimal growth for the first 24 to 48 h but logarithmically expands thereafter until bacteria exit or lyse the cells (46, 47). We previously detected *ank13* transcript by RT-PCR in cells in which the infection had become asynchronous (29). Whether *ank13* expression varies over the course of infection was unknown. Total RNA isolated from synchronously infected HeLa cells at 2, 4, 8, 24, 48, and 72 h was analyzed by RT-qPCR for *ank13* expression normalized to that of *O. tsutsugamushi* 16S rRNA (*ott16S*). Monitoring *ott16S*-to-*GAPDH* expression supported that, consistent with previous reports (46, 47), the bacterial population did not begin to expand until around 48 h (Fig. 2A). Though *ank13* expression was detected at all time points, significantly higher expression was observed at 48 and 72 h (Fig. 2B), suggesting that *O. tsutsugamushi* upregulates *ank13* during its expansive replication phase.

Ank13 is expressed and localizes to the nucleus in *O. tsutsugamushi*-infected cells. To verify that *O. tsutsugamushi* expresses Ank13 during infection, we generated Ank13-specific antiserum. Through *in silico* analyses, residues 288 to 360 within the ISR were determined to be unique to Ank13 within the Ikeda strain proteome. Rat antiserum specific for this region, here referred to as anti-Ank13, detected Flag-Ank13 in the nuclei and cytoplasm of transfected HeLa cells but did not recognize Flag-tagged BAP or Ank9 (Fig. 3A and B). Anti-Ank13 was then used to screen Western-blotted lysates of uninfected HeLa cells or cells that had been infected with *O. tsutsugamushi* at a

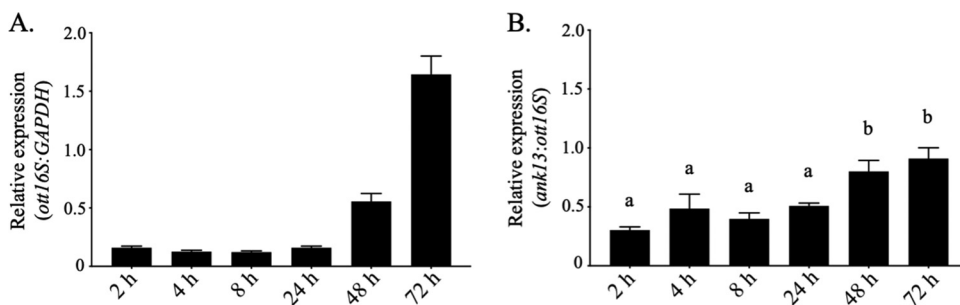


FIG 2 *O. tsutsugamushi* expresses *ank13* during infection of host cells. HeLa cells were synchronously infected with *O. tsutsugamushi*, followed by collection of total RNA at the indicated time points. RT-qPCR was performed using gene-specific primers. Relative *O. tsutsugamushi* 16S rRNA gene (*ott16S*)-to-human *GAPDH* (A) and *ank13*-to-*ott16S* expression (B) was determined using the $2^{-\Delta\Delta CT}$ method. The data are mean values \pm the SD from three experiments performed in triplicate. One-way ANOVA with Tukey's *post hoc* test was used to test for significant difference of relative *ank13* levels across time points. The mean values indicated by the letter "a" are significantly different from those labeled "b."

multiplicity of infection (MOI) of 10 for 24, 48, or 72 h or an MOI of 10, 20, or 50 for 72 h (Fig. 3C and D). Infection was verified by screening the blots with antiserum targeting TSA56 (56-kDa type-specific antigen), an abundantly expressed *O. tsutsugamushi* outer membrane protein (50). Anti-Ank13 recognized a band having an apparent molecular weight slightly below that of the 53.7-kDa size expected for Ank13 in lysates from infected, but not uninfected cells. Anti-Ank13 also detected a comparably sized band in cytosolic and nuclear fractions of infected cells (Fig. 3E). The signal intensity of the Ank13 band increased in both fractions over the 72-h time course, whereas a nonspecifically recognized host cell-derived band did not. Detection of TSA56 at a lower signal intensity in nuclear fractions relative to cytoplasmic fractions from infected cells at each time point is consistent with intranuclear localization of a subpopulation of *O. tsutsugamushi* organisms (51). Hence, *O. tsutsugamushi*-expressed Ank13 is present in both the cytoplasm and the nuclei of infected cells.

Ank13 interacts with the SCF ubiquitin ligase complex in an F-box-dependent manner and its nucleotropism is independent of the classical nuclear import pathway. We sought to confirm the ability of Ank13 to interact with SCF ubiquitin ligase machinery and to determine whether it translocates into the nucleus via the classical nuclear import pathway by focusing on the contributions of its C-terminal F-box and putative N-terminal nuclear localization signal (NLS), respectively. cNLS Mapper (52) identified Ank13 residues 10 through 41 as harboring a potential NLS by assigning the region a score of 7 out of a possible 10. Eukaryotic NLS-bearing cargo are delivered into the nucleus by the classical nuclear import pathway, which involves importin α recognition of the NLS, followed by binding of importin β 1 to importin α and importin β 1-mediated translocation of the ternary complex through the nuclear pore (53). To evaluate the putative NLS, we generated a construct encoding Flag-Ank13₄₉₋₄₉₀, which lacks through the end of the first AR (Fig. 4A). This deletion was necessary because the candidate NLS extends to within the first AR. Deleting part of an AR disrupts tertiary structure of an AR domain, but deleting an entire AR does not (54). The Ank13 F-box consists of residues 451 to 471 (Fig. 1A). We previously demonstrated that Flag-Ank13 but not Flag-Ank13 _{Δ 451-490}, here simply referred to as Flag-Ank13 Δ F-box (Fig. 4A), precipitated glutathione *S*-transferase-tagged Skp1 (30). Whether the Ank13 F-box is capable of interacting with endogenous Skp1 or any other SCF component was unknown. HeLa cells were transfected to express Flag-tagged Ank13, Ank13₄₉₋₄₉₀, or Ank13 Δ F-box. Lysates were collected and incubated with Flag antibody-coated beads to immunoprecipitate the Flag-tagged proteins and their interacting partners. Eluted complexes were Western blotted and screened with antibodies for Skp1, Cul1, and Rbx1. Flag-Ank13 and Flag-Ank13₄₉₋₄₉₀, but not Flag-Ank13 Δ F-box, coprecipitated all three (Fig. 4B), thereby confirming that Ank13 interacts with the

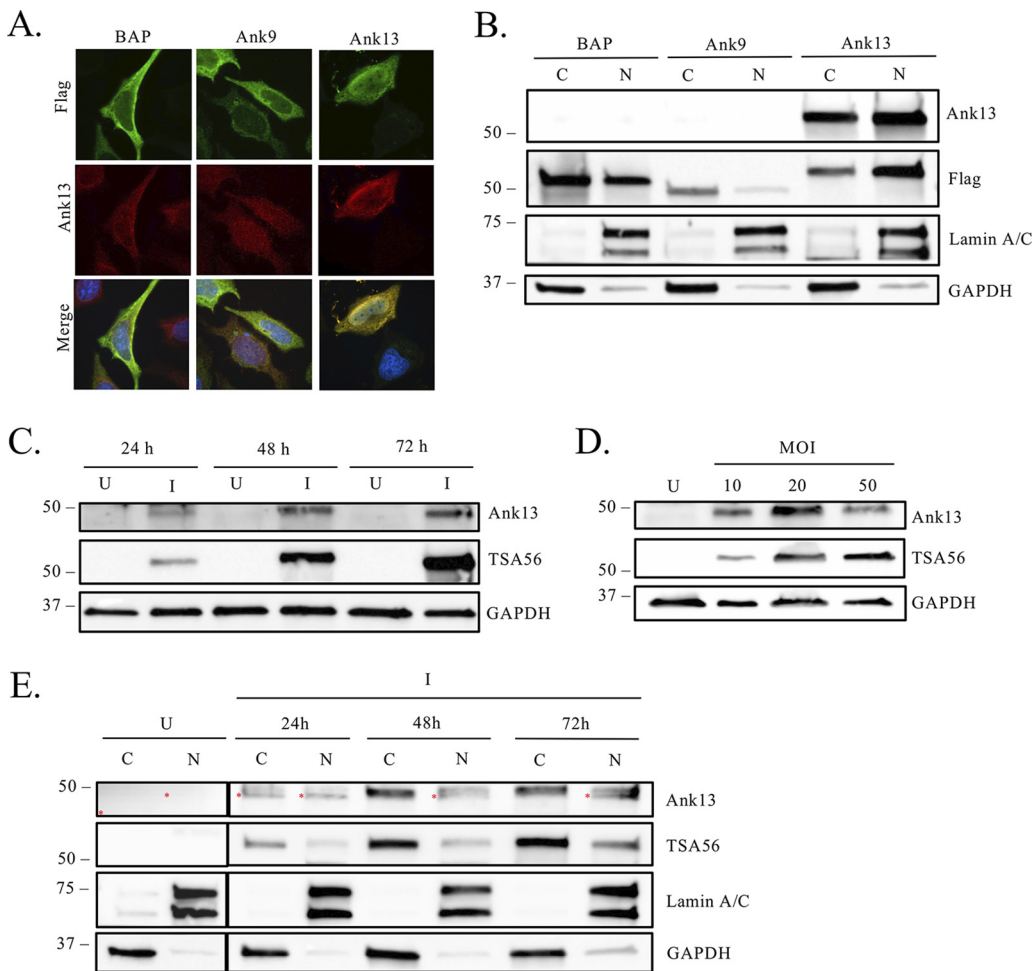


FIG 3 Antiserum specific for Ank13₂₈₈₋₃₆₀ detects ectopically expressed and *O. tsutsugamushi* Ank13 in infected cells. (A and B) Anti-Ank13₂₈₈₋₃₆₀ (anti-Ank13) specifically recognizes Flag-Ank13. HeLa cells expressing Flag-tagged BAP, Ank9, or Ank13 were either (i) fixed, probed with anti-Flag and anti-Ank13, stained with DAPI, and examined by immunofluorescence microscopy (A) or (ii) lysed and separated into cytoplasmic [C] and nuclear [N] fractions that were subjected to Western blot analyses using lamin A/C, GAPDH, Ank13, and Flag epitope antibodies (B). (C to E) Anti-Ank13 detects bacterium-derived Ank13 in *O. tsutsugamushi*-infected cells. HeLa cells were either mock [U] or infected [I] with *O. tsutsugamushi* at an MOI of 10, and whole-cell lysates were collected at 24, 48, and 72 h (C). An MOI of 10, 20, or 50 and whole-cell lysates was collected at 72 h (D), or an MOI of 10 and cytoplasmic [C] and nuclear [N] fractions was collected at 24, 48, and 72 h (E). Western blots were probed with the indicated antibodies. Red asterisks in panel E denote nonspecific host cell-derived bands. The results are representative of at least three experiments with similar results.

endogenous SCF complex in an F-box-dependent manner. Subcellular distribution of Flag immunosignal, as analyzed by both indirect immunofluorescence and Western blotting, demonstrated that Flag-Ank13, Flag-Ank13_{49-490r}, and Flag-Ank13 Δ F-box exhibited comparable accumulation in the nucleus (Fig. 4C to E). Hence, the Ank13 nucleotropism requires neither Ank13 residues 1 through 48 nor its F-box. Moreover, Ank13 residues 10 through 41 do not contain an NLS.

To further confirm that Ank13 translocation into the nucleus occurs independently of classical nuclear import, HeLa cells expressing Flag-tagged Ank13, Ank6, or Ank9 were treated with importazole, a small molecular inhibitor of importin β 1 (55), or DMSO vehicle followed by assessment of Flag immunosignal accumulation in the nucleus. As previously reported (16), importazole inhibited Ank6 nuclear translocation but had no effect on Ank9. Flag-Ank13 subcellular localization was comparable between both conditions (Fig. 5A and B). As an additional control to verify the efficacy of importazole treatment, its effect on nuclear import of NLRC5 (NOD-like receptor

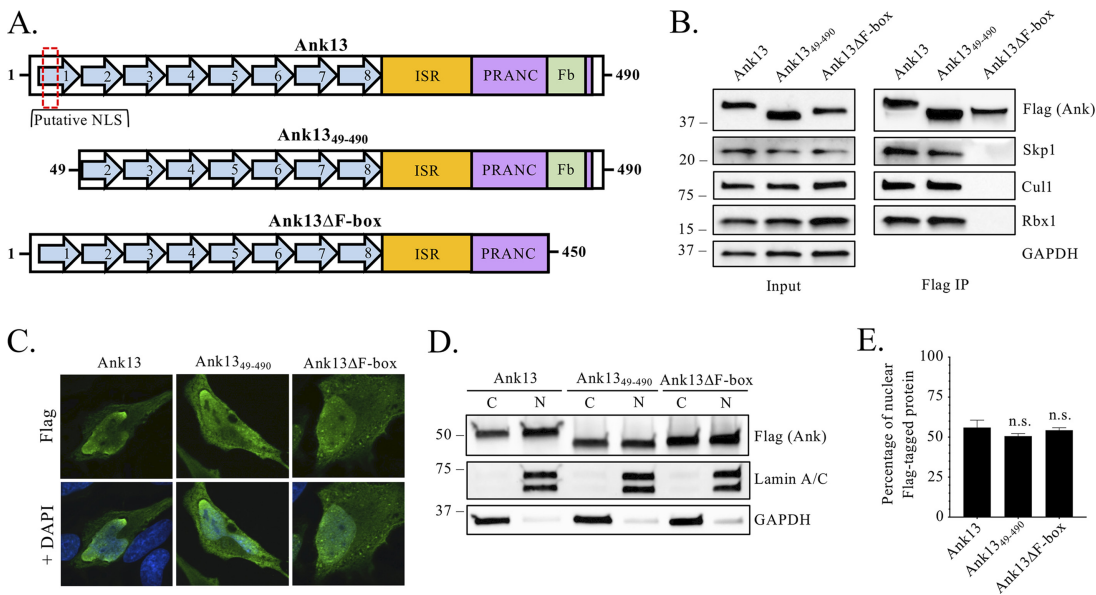


FIG 4 A putative NLS does not contribute to Ank13 nucleotropism. (A) Schematics of wild-type and Ank13 truncated mutant proteins. A red hatched line box indicates the putative NLS that consists of residues 10 to 42 and occurs within ankyrin repeat 1. (B) Confirmation that Ank13ΔF-box fails to interact with SCF ubiquitin ligase components. HeLa cells were transfected to express Flag-tagged Ank13, Ank13₄₉₋₄₉₀, or Ank13ΔF-box. Input lysates were subjected to Western blotting with Flag antibody to verify ectopic expression of the proteins of interest; antibodies against Skp1, Cul1, and Rbx1 to confirm their presence; and GAPDH antibody to validate that equivalent amounts of protein were present in each sample. Whole-cell lysates were incubated with Flag antibody-conjugated agarose beads to immunoprecipitate (IP) Flag-tagged proteins and their interacting proteins. The resulting Western blot was probed with indicated antibodies to confirm recovery of the Flag-tagged proteins and assess for Skp1, Cul1, or Rbx1 coimmunoprecipitation. (C to E) Ankyrin repeat 1 (containing the putative NLS) and the F-box of Ank13 are dispensable for nuclear localization. Transfected HeLa cells expressing Flag-Ank13, Flag-Ank13₄₉₋₄₉₀, or Flag-Ank13ΔF-box were either fixed, probed with Flag antibody, stained with DAPI, and examined by immunofluorescence microscopy (C) or lysed and resolved into cytoplasmic [C] and nuclear [N] fractions that were subjected to Western blot analyses using the indicated antibodies (D). (E) The nuclear densitometric value was divided by the sum of nuclear and cytoplasmic densitometric values for Flag-tagged proteins in panel D. The quotient was multiplied by 100 to yield the percentage of Flag-tagged protein in the nucleus. Data presented are the percentages (means ± the SD) of Flag-tagged proteins exhibiting nuclear localization from three separate experiments. One-way ANOVA with Tukey's *post hoc* test was used to assess for significant differences among the conditions. n.s., not significant.

family CARD domain containing 5), a eukaryotic transcription factor that shuttles into the nucleus by virtue of its NLS (56), was examined. HeLa cells were stimulated with gamma interferon (IFN-γ) to increase NLRC5 expression, followed by importazole treatment and nuclear fractionation. A clear reduction of nuclear NLRC5 in importazole treated cells was observed (see Fig. S3). Finally, transfected HeLa cells expressing Flag-tagged Ank6, Ank9, or Ank13 were treated with importazole, followed by nuclear fractionation and Western blot analyses. Importazole treatment inhibited Ank6 nuclear accumulation but had no effect on the nonspecific low-level nuclear accumulation of Ank9 (Fig. 5C). Ank13 was as abundant in the nuclear fractions of importazole-treated cells as in those of control cells. Overall, Ank13 does not enter the nucleus via the classical nuclear import pathway.

RaDAR-mediated nuclear import of Ank13 requires isoleucine 127. The RaDAR pathway is an importin-independent nuclear import route by which eukaryotic AR-containing proteins bind RanGDP to be delivered into the nucleus. RanGDP binding requires that one or two, often consecutive, ARs contain a hydrophobic residue—preferentially L, I, or F—or C at the 13th position (57). Ank13 ARs two through five have the following hydrophobic residues at the thirteenth position: AR2 V62, AR3 A95, AR4 I127, and AR5 I161 (Fig. 6A). The study that discovered RaDAR also found that substituting the key hydrophobic AR residues with hydrophilic R strongly disrupted nuclear translocation, while swapping in L or I was less disruptive (57). Flag-Ank13_{1127R} delivery into the nucleus was all but abolished and Flag-Ank13_{1127L} nuclear translocation was lowered by approximately 40% relative to Flag-Ank13 (Fig. 6B). By comparison, Flag-

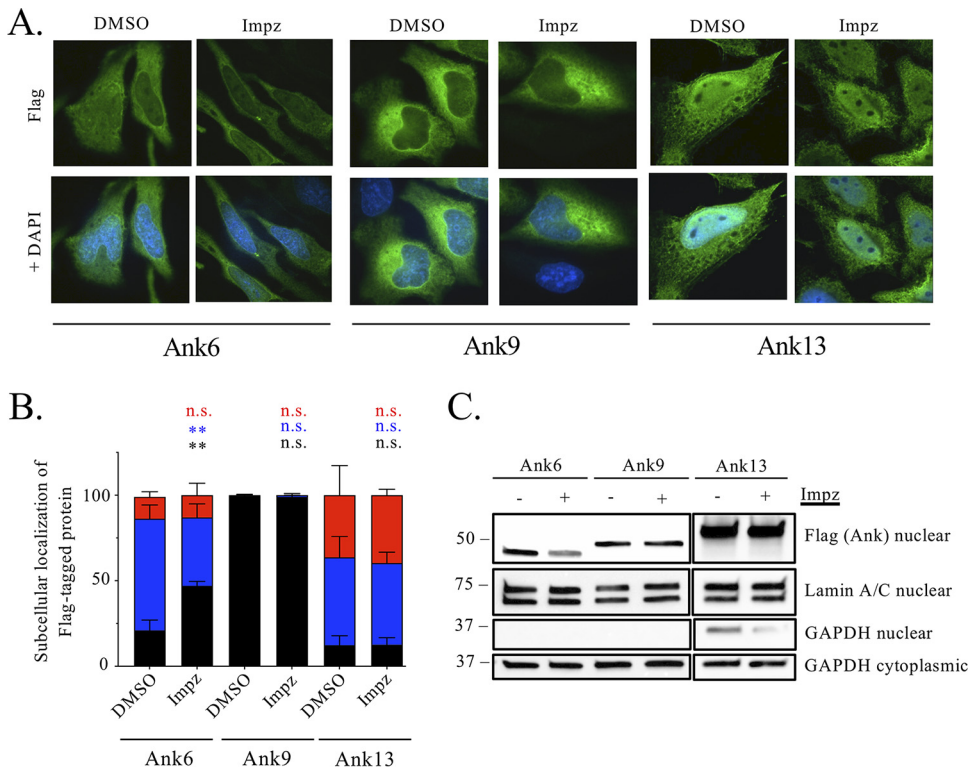


FIG 5 Ank13 nuclear accumulation is importazole-insensitive. HeLa cells expressing Flag-tagged Ank6, Ank9, or Ank13 were treated with importazole (Impz) or DMSO for 3 h and then fixed, probed with Flag antibody, stained with DAPI, and examined by immunofluorescence microscopy. (A) Representative immunofluorescent images. (B) One hundred cells per condition were examined in triplicate to quantify the percentages (means \pm the SD) of cells exhibiting Flag immunosignal subcellular localization, scored as being exclusively cytoplasmic (black), throughout the cell (blue), or exclusively in the nucleus (red). Two-way ANOVA with Dunnett's correction was used to determine significance between subcellular locations of Flag-Ank13 in cells treated with Impz versus DMSO. (C) Transfected HeLa cells were separated into cytoplasmic [C] and nuclear [N] fractions that were subjected to Western blot analyses using Flag antibody to verify Flag-tagged protein expression and antibodies against lamin A/C and GAPDH to confirm fraction purity. The data are representative of three experiments with similar results. Statistically significant values are indicated. **, $P < 0.01$; n.s., not significant.

tagged Ank13_{V62R}, Ank13_{A95R}, and Ank13_{I161R} exhibited more modest reductions in nuclear import efficiency. Due to the essentiality of AR4 I127 for Ank13 nuclear import, because efficient RaDAR-mediated nuclear import of eukaryotic AR-containing transcription factors is reliant on hydrophobic residues at the 13th position in two consecutive ARs (57), and because said 13th positions tend to be more commonly occupied by I than A (57), we examined the nuclear translocation efficiency of Flag-Ank13_{I127RI161R}. Though the nuclear translocation defect of Flag-Ank13_{I127RI161R} was slightly stronger than for Flag-Ank13_{I127R}, the difference was statistically insignificant (Fig. 6C to E). This was most likely due to the overwhelming inhibitory effect of the I127R versus I161R mutation. Thus, Ank13 AR4 I127 and AR5 I161 are critical and contributory, respectively, for its ability to coopt the RaDAR pathway for transport into the nucleus.

The ability of Ank13 to interfere with yeast growth requires nuclear translocation and the F-box domain. Toxicity screens using *Saccharomyces cerevisiae* as a model are useful for studying bacterial effectors due to the high degree of conservation of cellular processes between yeast and mammalian cells. To determine whether Ank13 is toxic to yeast and, if so, whether its ability to translocate into the nucleus and its F-box contribute to its toxicity, Ank13, Ank13_{I127R}, and Ank13 Δ F-box were inserted into the galactose-inducible vector pYesNTA2. *S. cerevisiae* W303 transformed with these constructs was grown in uracil dropout media, serially diluted 10-fold, and spotted onto dropout agar containing 2% glucose or 2% galactose. Yeast carrying empty vector or the toxic *Chlamydia trachomatis* effector CT694 served as negative and positive controls, respectively. Ank13 interfered with yeast growth as severely as CT694 (Fig. 7).

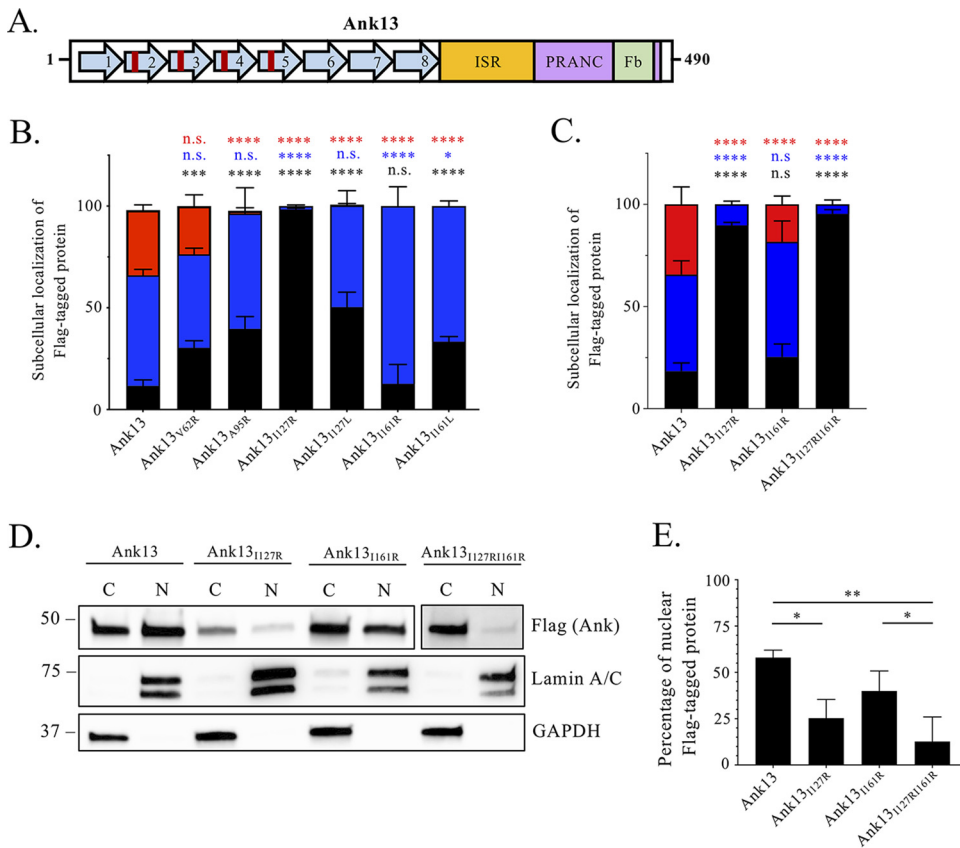


FIG 6 Iso127 and Iso161 are critical for and contribute to Ank13 nuclear localization. (A) Schematic of Ank13 with the relative positions of V62, A95, I127, and I161 denoted as red lines. These amino acids were replaced with R or L to generate indicated mutants. (B to E) Transfected HeLa cells expressing Flag-Ank13 or Flag-Ank13 bearing the indicated amino acid substitutions were either examined by immunofluorescence microscopy (B and C) or Western blot analysis of nuclear [N] and cytoplasmic [C] fractions (D and E). (B and C) One hundred cells were examined per condition in triplicate to quantify the percentages (means \pm the SD) of cells exhibiting Flag immunosignal localization, which was scored as being exclusively cytoplasmic (black), throughout the cell (blue), or exclusively in the nucleus (red). Two-way ANOVA with Dunnett's correction determined significance between subcellular locations of Flag-tagged proteins compared to Flag-Ank13. (D) Western-blotted cytoplasmic [C] and nuclear [N] fractions were probed with lamin A/C and GAPDH antibody to verify fraction purity and Flag antibody to determine localization of Flag-tagged protein. (E) The densitometric value of each Flag-tagged protein in the nucleus was divided by the sum of the densitometric values for nuclear and cytoplasmic signals in panel D. The quotient was multiplied by 100 to yield the percentage of Flag-tagged protein in the nucleus. Data presented are the means \pm the SD percentage of Flag-tagged proteins exhibiting nuclear localization from three separate experiments. One-way ANOVA with Tukey's *post hoc* test was used to assess for significant differences among the conditions. *, $P < 0.05$; **, $P < 0.01$; ***, $P < 0.001$; ****, $P < 0.0001$. n.s., not significant.

Toxicity was reduced in yeast expressing Ank13_{I127R} and abrogated in yeast expressing Ank13 Δ F-box. Thus, Ank13 modulates critical eukaryotic biological processes via a mechanism that involves its nucleotropism and requires its ability to interact with host cell ubiquitin ligase components.

Ank13 alteration of host cell gene expression is nuclear trafficking dependent, F-box dependent, and F-box independent. Tools for genetically manipulating *O. tsutsugamushi* are lacking. As an alternative approach to determine whether Ank13 dysregulates host cell gene expression and assess whether such ability involves its nucleotropism and/or F-box domain, transfected HeLa cells expressing GFP-Ank13, GFP-Ank13_{I127R}, GFP-Ank13 Δ F-box, or GFP were sorted based on GFP positivity (see Fig. S4) followed by total RNA isolation and RNAseq. Differential gene expression in cells expressing GFP-tagged Ank13, Ank13_{I127R}, or Ank13 Δ F-box versus GFP was calculated as log₂(fold change) based on negative binomial distribution (58). Ank13, Ank13 Δ F-box, and Ank13_{I127R} promoted differential expression of 2012, 2836, and 249 host genes,

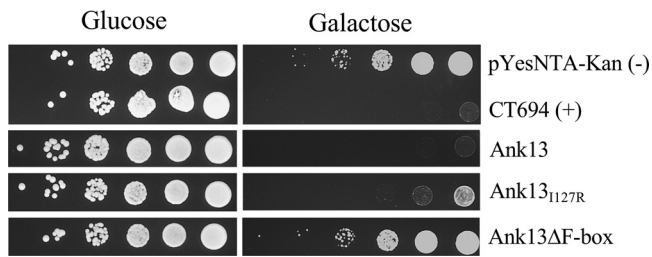


FIG 7 Ank13 interferes with yeast growth in a nuclear translocation- and F-box-dependent manner. *S. cerevisiae* W303 was transformed with pYesNTA-Kan constructs for expressing *C. trachomatis* CT694, Ank13, Ank13_{1127R}, Ank13ΔF-box, or vector alone. Transformants were diluted to an optical density at 600 nm of 0.2 and spotted as 10-fold serial dilutions onto dropout media containing 2% glucose (noninducing conditions) or 2% galactose (inducing conditions). The data are representative of two to four experiments with similar results.

respectively (Fig. 8; see also Data Set S1 in the supplemental material). Although Ank13 and Ank13ΔF-box similarly dysregulated 870 genes, the majority of transcriptional changes influenced by each were specific to either protein (Fig. 8A; see also Data Set S1). Only 10 genes were altered in an Ank13_{1127R}-specific manner (Fig. 8A; see also Data Set S1). Selecting genes exhibiting at least a 2-fold change in expression among the three transfected populations revealed that the majority were downregulated (Fig. 8B to D; see also Data Set S2). Thus, Ank13 is predominantly a negative regulator of host cell gene expression. While its ability to modulate gene expression primarily relies on its translocation into the nucleus, Ank13 exerts its influence in both F-box-dependent and -independent manners.

Gene ontology (GO) terms were assigned to all differentially regulated genes in cells expressing GFP-Ank13, GFP-Ank13_{1127R} or GFP-Ank13ΔF-box (see Data Set S3). The top 20 GO biological processes up- or downregulated per effector as determined by the $-\log_{10}(P_{\text{adj}})$ value are presented in Fig. 9. The two largest categories of genes downregulated by GFP-Ank13 and GFP-Ank13ΔF-box were histone modification and covalent chromatin modification (Fig. 9A and C; see also Fig. S5A and C). Both proteins also downregulated genes associated with histone methylation. All of the remaining top 20 biological processes downregulated by GFP-Ank13ΔF-box were also downregulated by GFP-Ank13 (Fig. 9A and C; see also Data Set S3). Other major categories of genes downregulated by GFP-Ank13 included those associated with regulation of chromatin organization, nuclear division, positive regulation of cell adhesion, and hemopoiesis (Fig. 9A; see also Fig. S5A). From these data it can be concluded that, while Ank13 negatively modulates expression of genes associated with a variety of biological processes, it especially targets those associated with epigenetic functions and does so independently of its F-box.

The largest two categories of genes upregulated in GFP-Ank13-expressing cells were mRNA and RNA catabolic processes, followed by protein targeting to membranes, especially the endoplasmic reticulum (ER) (Fig. 9B; see also Fig. S5B). Of the top 20 most upregulated GO processes, 12 fell into these and similar categories (Fig. 9B). The top 20 biological processes transcriptionally upregulated by GFP-Ank13ΔF-box were also upregulated by GFP-Ank13 (Fig. 9B and D; see also Fig. S5B and D and Data Set S3). However, whereas GFP-Ank13 upregulated 86 mRNA catabolism genes and 89 RNA catabolism genes (Fig. 9B), GFP-Ank13ΔF-box upregulated only 45 mRNA catabolism genes and no RNA catabolism genes (see Data Set S3). Transcriptional upregulation of ER/membrane-localization processes was also GFP-Ank13 specific. When the up- and downregulated pathways in cells expressing GFP-Ank13_{1127R} were examined, there were markedly fewer differentially expressed genes (Fig. 9E and F). The biological processes themselves were a clear departure from those modulated by GFP-Ank13 and GFP-Ank13ΔF-box, signifying that much of the Ank13 modulatory effect is linked to its nucleotropism (Fig. 9). The most upregulated genes included those associated with topologically incorrect or unfolded

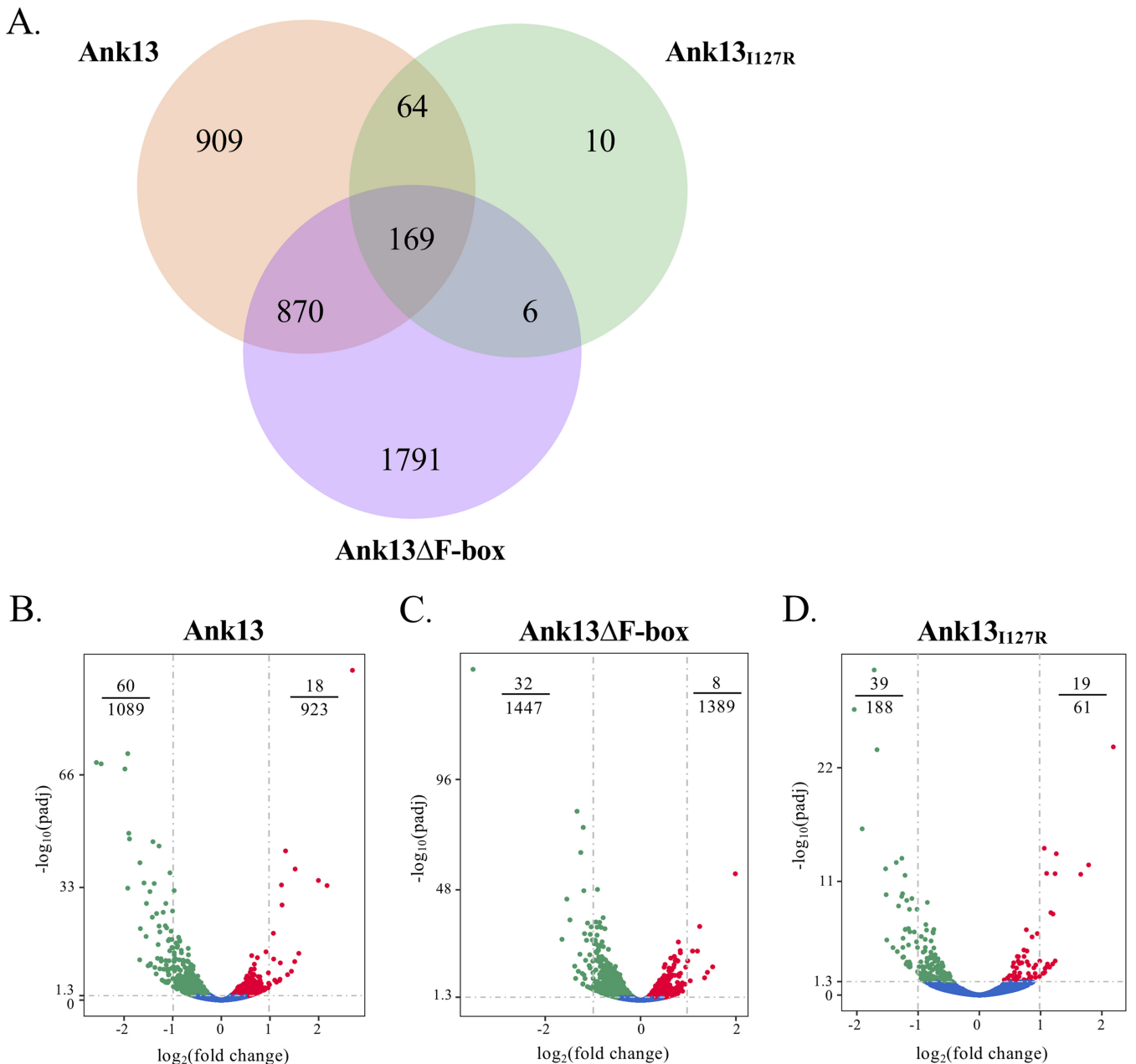
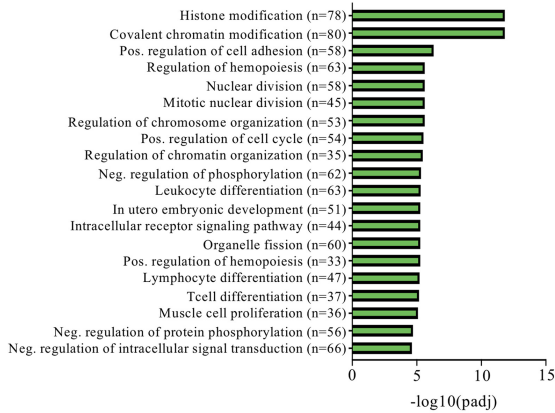


FIG 8 Differential gene expression profiles influenced by Ank13, Ank13_{I127R}, or Ank13ΔF-box. (A) Venn diagram showing unique and shared genes differentially expressed by Ank13 (orange, 2012 total), Ank13ΔF-box (purple, 2836 total), or Ank13_{I127R} (green, 249 total). The sum within each circle is the total number of differentially expressed genes in this group and overlapping regions show the number of common genes among comparison groups. (B to D) Volcano plots showing differential expression profiles for cells expressing GFP-tagged Ank13 (B), Ank13ΔF-box (C), or Ank13_{I127R} (D) compared to GFP. Gray horizontal dashed line indicates the threshold for significantly differentially expressed genes ($P_{adj} < 0.05$). Vertical dashes indicate genes exhibiting a $\log_2(\text{fold change})$ of >1 or <-1 . Each dot corresponds to an individual gene. Blue dots indicate no significant difference in expression for cells expressing GFP fusions compared to cells expressing GFP. Red and green dots indicate genes that are up- or downregulated, respectively, in cells expressing GFP-fusions versus cells expressing GFP. Fractions in top corners denote the number of genes with $\log_2(\text{fold change})$ of >1 or <-1 out of the total number of differentially expressed genes.

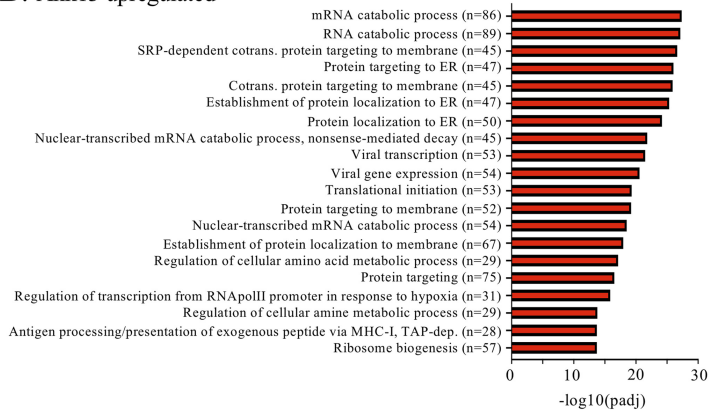
proteins, cellular stress, and apoptosis (Fig. 9E and F), suggesting that cytoplasmic accumulation of overexpressed GFP-Ank13_{I127R} invokes cellular stress responses.

Overall, the GO analyses demonstrate that, among the many host cellular processes that Ank13 transcriptionally modulates, it impairs expression of genes involved in epigenetic regulation in an F-box-independent manner and upregulates genes associated with mRNA/RNA catabolism and membrane/ER targeting primarily in an F-box-dependent manner. Both of these phenomena are predicated on the effector's nucleotropism.

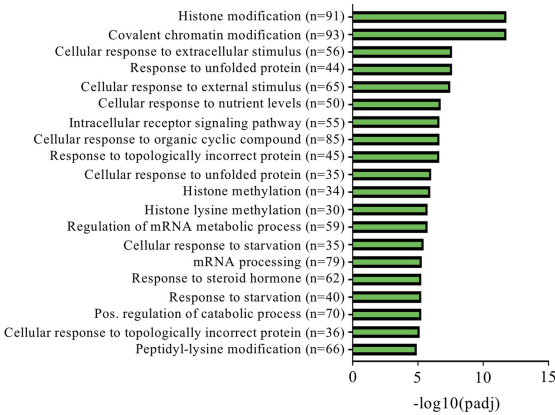
A. Ank13 downregulated



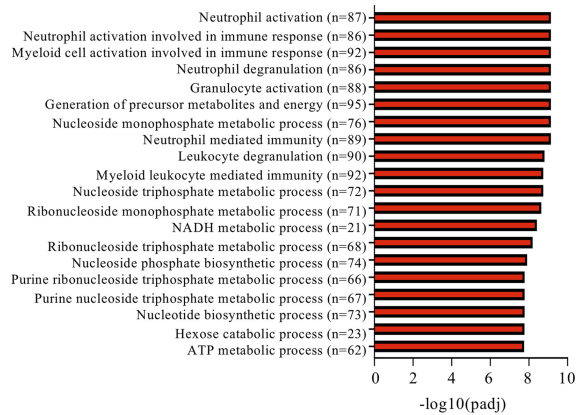
B. Ank13 upregulated



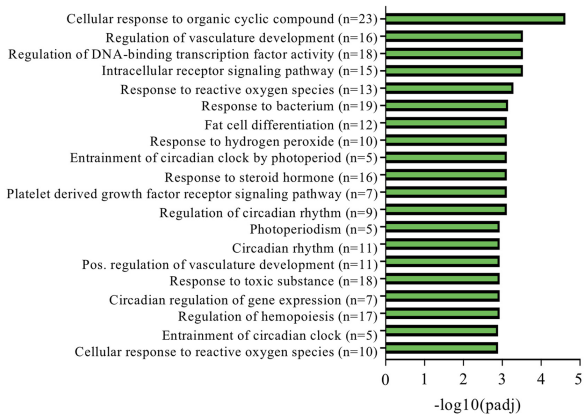
C. Ank13ΔF-box downregulated



D. Ank13ΔF-box upregulated



E. Ank13_{1127R} downregulated



F. Ank13_{1127R} upregulated

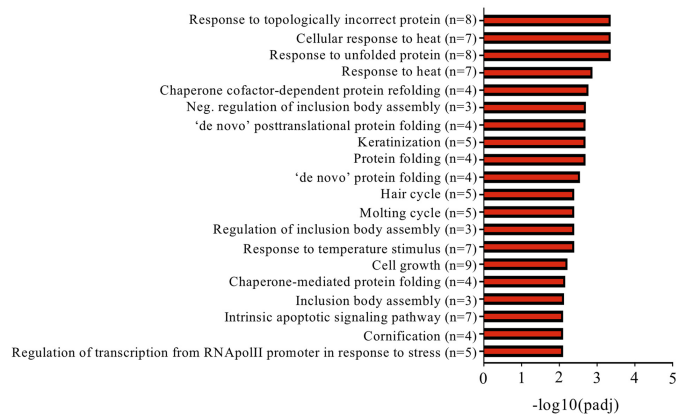


FIG 9 Differentially regulated pathways in cells expressing Ank13, Ank13_{1127R} or Ank13ΔF-box grouped by biological process. Bar plots showing the GO terms subdivided by biological processes that are down- or upregulated in cells expressing GFP-tagged Ank13 (A and B), Ank13ΔF-box (C and D), or Ank13_{1127R} (E and F) compared to cells expressing GFP. Shown are the top 20 most significantly enriched downregulated (green; A, C, and E) and upregulated (red; B, D, and F) GO terms as determined by $-\log_{10}(P_{adj})$ value. *n* = number of genes included in GO term.

Genes most strongly downregulated by Ank13 include those involved in transcriptional control and inflammation and correlate with transcriptional trends in *O. tsutsugamushi*-infected cells. Being that Ank13 is primarily a negative transcriptional modulator, we next focused on the 60 genes that were downregulated ≥ 2 -fold in cells expressing GFP-Ank13 (see Data Set S2). We categorized these genes as being downregulated dependent on Ank13 I127 and/or its F-box. Genes downregulated ≥ 2 -

fold in cells expressing GFP-Ank13, but neither GFP-Ank13_{1127R} nor GFP-Ank13ΔF-box were interpreted as being inhibited by Ank13 in both nucleotropism- and F-box-dependent manners. Genes meeting this criterion in cells expressing GFP-Ank13 and GFP-Ank13ΔF-box, but not GFP-Ank13_{1127R}, were considered to be negatively modulated by Ank13 in a nucleotropism-dependent but F-box-independent mechanism. Those downregulated in cells expressing GFP-Ank13 and GFP-Ank13_{1127R}, but not GFP-Ank13ΔF-box were regarded as being impaired by Ank13 in an F-box-dependent but nucleotropism-independent manner. Of the 60 genes, 46 were categorizable per these criteria (Table 1). Ank13 downregulates a total of 15 genes involved in transcriptional control in nucleotropism- and F-box-dependent, as well as -independent, fashions. It negatively modulates 15 proinflammatory genes, including NF- κ B-related genes in both nucleotropism- and F-box-dependent manners plus interleukin-1 α (IL-1 α), IL-1 receptor-associated kinase 2, tumor necrosis factor-related genes, and NF- κ B inhibitor α via an F-box-dependent mechanism. Supporting this trend, STRING (Search Tool for the Retrieval of Interacting Genes/Proteins) (59) analysis of genes downregulated ≥ 2 -fold by GFP-Ank13 revealed a functional enrichment for the inflammatory response (Fig. 10A). The effector uses its F-box independent of its nucleotropism to downregulate genes involved in cell cycle control, interferon response, mRNA, and histone deacetylase nine. Ank13 also traffics to the nucleus to inhibit transcription of histone cluster and heat shock protein family A genes in an F-box-independent manner. In contrast and as further evidence that Ank13 predominantly acts to transcriptionally downregulate numerous interrelated host cell processes, STRING analysis of genes upregulated ≥ 2 -fold by GFP-Ank13 showed little functional enrichment aside from a few that are involved in keratinization (Fig. 10B).

To assess for correlations between expression profiles induced by GFP-Ank13 and *O. tsutsugamushi* infection, RNA-seq was performed on HeLa cells that had been infected for 4 or 48 h, the latter time point corresponding to when Ank13 is detectable by Western blotting. Host gene expression in infected cells was measured relative to uninfected controls. There was an ~ 4 -fold increase in the number of differentially expressed genes at 48 h versus 4 h (Fig. 11; see also Data Set S2). Included in the top 20 GO biological processes upregulated at 4 or 48 h were genes involved in recognition of and response to pathogens, cell proliferation, positive regulation of the mitogen-activated protein kinase cascade, and negative regulation of protein phosphorylation (see Data Set S3). Most of the genes downregulated at 4 h were associated with cell differentiation (see Data Set S3). Consistent with *O. tsutsugamushi* countering immune processes, genes downregulated at 48 h included those involved in leukocyte activation, antigen processing, and antigen presentation (see Data Set S3). The most striking observation was that of the 46 genes that GFP-Ank13 inhibits ≥ 2 -fold, 40 were either not expressed at both infection time points or were more downregulated at 48 h than 4 h (Table 1). Indeed, aligned with prior reports that *O. tsutsugamushi* stimulates the NF- κ B response initially following invasion but then actively represses it as infection proceeds (16, 20), NFKB1 and NFKB2 were among several genes upregulated at 4 h but downregulated at 48 h. Overall, the majority of the genes that GFP-Ank13 most strongly represses, which include those involved in transcriptional regulation and the inflammatory response, are either quiescent or downregulated in *O. tsutsugamushi* infected cells at a time point when the bacterium expresses Ank13. We conclude that Ank13 contributes to the pathogen's ability to transcriptionally modulate host cell responses during infection.

DISCUSSION

Intracellular bacteria use secreted effectors that coopt, subvert, and manipulate eukaryotic processes to generate niches inside host cells. The expansive role of nucleomodulins in this approach has only recently begun to be realized. By targeting host cells at the transcriptional level, nucleomodulins have the capacity to globally alter any number of cellular responses to facilitate microbial colonization (1, 2). This strategy is

TABLE 1 Host genes downregulated ≥ 2 -fold in cells expressing GFP-Ank13 proteins correlated with their transcriptional profiles in *O. tsutsugamushi* infected cells^a

| Biological group | Gene | Description | Location | Cells expressing GFP-Ank13 proteins | | | <i>O. tsutsugamushi</i> -infected cells | | |
|--|--|--|--|-------------------------------------|-----------------------------|------------------------------|---|----------------------------|----|
| | | | | Wild-type log ₂ (FC) | I127R log ₂ (FC) | ΔF-box log ₂ (FC) | 4 h log ₂ (FC) | 48 h log ₂ (FC) | |
| Downregulation is nucleotropism and F-box-dependent Transcriptional control | ELF3 | E74-like factor 3 (Ets domain transcription factor epithelium-specific) | Nucleus | -1.22 | NC ^b | NC | NC | NC | |
| | BCOR | BCL6 corepressor | Nucleus | -1.02 | -0.74 | NC | NC | NC | |
| | HES1 | Hes family bHLH transcription factor 1 | Nucleus | -1.20 | -0.67 | -0.63 | NC | NC | |
| | BHLHE40 | Basic helix-loop-helix family member e40 | Nucleus | -1.06 | -0.48 | -0.19 | NC | 0.64 | |
| | PRDM1 | PR domain containing 1 with ZNF domain | Nucleus | -1.26 | NC | -0.66 | NC | 1.14 | |
| | BDKRB1 | Bradykinin receptor B1 | Plasma membrane | -1.46 | NC | NC | NC | -1.27 | |
| | CYLD | Cylindromatosis (turban tumor syndrome) | Plasma membrane, cytoplasm | -1.06 | -0.78 | -0.54 | NC | NC | |
| | REL | v-rel avian reticuloendotheliosis viral oncogene homolog | Nucleus | -1.46 | NC | -0.57 | NC | NC | |
| | NFKBIE | Nuclear factor of kappa light polypeptide gene enhancer in B cells inhibitor epsilon | Cytoplasm | -1.10 | NC | NC | NC | NC | |
| | NFKB1 | Nuclear factor of kappa light polypeptide gene enhancer in B cells 1 | Nucleus, cytoplasm | -1.14 | -0.86 | -0.50 | 0.41 | NC | |
| | NFKB2 | Nuclear factor of kappa light polypeptide gene enhancer in B cells 2 (p49/p100) | Nucleus, cytoplasm | -1.41 | -0.74 | -0.48 | 0.65 | NC | |
| | Downregulation is F-box dependent Transcriptional control | CSRNP1 | Cysteine-serine-rich nuclear protein 1 | Nucleus | -1.38 | -1.27 | -0.81 | NC | NC |
| | | TEF | Thyrotrophic embryonic factor | Nucleus | -1.18 | -1.21 | NC | NC | NC |
| | | HIVEP2 | Human immunodeficiency virus type 1 enhancer binding protein 2 | Nucleus | -1.28 | -0.91 | -0.68 | NC | NC |
| ZFP36 | | ZFP36 ring finger protein | Nucleus | -1.08 | -0.95 | -0.79 | NC | NC | |
| KLF10 | | Kruppel-like factor 10 | Nucleus | -1.28 | -1.02 | -0.68 | NC | NC | |
| ZNF620 | | Zinc finger protein 620 | Nucleus | -1.08 | -0.89 | NC | NC | NC | |
| LBX2-AS1 | | LBX2 antisense RNA 1 | Nucleus | -1.08 | -1.01 | -0.48 | NC | NC | |
| Inflammatory response | IL1A | IL-1 α | Extracellular | -1.08 | -1.01 | -0.43 | NC | NC | |
| | IRAK2 | IL-1 receptor associated kinase 2 | Plasma membrane, extracellular, cytoskeleton, nucleus | -1.59 | -1.14 | NC | 1.21 | NC | |
| | TNF | Tumor necrosis factor | Plasma membrane, extracellular | -1.34 | -1.41 | NC | NC | NC | |
| | TRAF1 | TNF receptor-associated factor 1 | Plasma membrane, cytoplasm | -2.57 | -2.04 | -0.76 | NC | NC | |
| | TNFAIP2 | TNF alpha-induced protein 2 | Extracellular | -1.47 | -1.36 | -0.39 | NC | NC | |
| | TNFAIP3 | TNF alpha induced protein 3 | Nucleus, lysosome | -1.98 | -1.53 | -0.68 | NC | NC | |
| | NUAK2 | NUAK family SNF1-like kinase 2 | Nucleus | -1.30 | -1.25 | -0.57 | NC | NC | |
| | NFKBIA | Nuclear factor of kappa light polypeptide gene enhancer in B cells inhibitor alpha | Nucleus (cytoplasm) | -1.67 | -1.03 | -0.39 | NC | NC | |
| | BIRC3 | Baculoviral IAP repeat containing 3 | Nucleus | -1.90 | -1.16 | -0.30 | NC | NC | |

(Continued on next page)

TABLE 1 (Continued)

| Biological group | Gene | Description | Location | Cells expressing GFP-Ank13 proteins | | | O. tsutsugamushi-infected cells | |
|---|-----------|---|---|-------------------------------------|-----------------------------|------------------------------|---------------------------------|----------------------------|
| | | | | Wild-type log ₂ (FC) | I127R log ₂ (FC) | ΔF-box log ₂ (FC) | 4 h log ₂ (FC) | 48 h log ₂ (FC) |
| IFN response | IRF1 | Interferon regulatory factor 1 | Nucleus | -1.54 | -1.27 | -0.59 | NC | NC |
| | IFIT2 | Interferon induced protein with tetratricopeptide repeats 2 | Endoplasmic reticulum | -1.12 | -0.95 | NC | NC | 2.49 |
| mRNA | FAM46B | Family with sequence similarity 46 member B | Cytoskeleton, nucleus | -1.10 | -1.13 | -0.59 | -0.63 | -1.98 |
| | NOCT | Nocturnin | Cytoskeleton | -0.97 | -1.10 | -0.62 | NC | NC |
| Histone deacetylase | HDAC9 | Histone deacetylase 9 | Nucleus | -1.19 | -0.92 | NC | NC | NC |
| | ADIRF-AS1 | ADIRF antisense RNA 1 | Nucleus | -1.55 | -1.25 | -0.87 | NC | NC |
| Cell cycle control | NR1D2 | Nuclear receptor subfamily 1 group D member 2 | Nucleus | -1.12 | -1.16 | -0.50 | NC | NC |
| | FAM214A | Family with sequence similarity 214 member A | Nucleus | -1.24 | -0.93 | -0.74 | NC | NC |
| Downregulation is nucleotropism-dependent | PER2 | Period circadian clock 2 | Nucleus | -1.24 | -0.96 | NC | NC | NC |
| | PER1 | Period circadian clock 1 | Nucleus | -1.92 | -1.72 | -0.83 | NC | 0.52 |
| Transcriptional control | NR1D1 | Nuclear receptor subfamily 1 group D member 1 | Nucleus | -1.92 | -1.91 | -0.43 | NC | 0.69 |
| | DUSP8 | Dual specificity phosphatase 8 | Nucleus | -1.09 | -0.71 | -1.13 | NC | -1.12 |
| Heat shock proteins | NR4A2 | Nuclear receptor subfamily 4 group A member 2 | Nucleus | -1.15 | -0.77 | -0.95 | -0.57 | NC |
| | C11orf96 | Chromosome 11 open reading frame 96 | NC | -1.14 | NC | -0.94 | NC | 1.94 |
| Histone cluster | HSPA1A | Heat shock protein family A (Hsp70) member 1A | Cytoskeleton, nucleus | -0.66 | 1.20 | -1.11 | NC | -0.63 |
| | HSPA1B | Heat shock protein family A (Hsp70) member 1B | Cytoskeleton | -0.86 | 1.06 | -1.19 | NC | NC |
| Histone cluster | HSPA6 | Heat shock protein family A (Hsp70) member 6 | Plasma membrane, cytoskeleton, nucleus, extracellular | -2.47 | 0.81 | -3.51 | NC | NC |
| | HIST1H1C | Histone cluster 1 H1c | Nucleus | -0.73 | NC | -1.27 | NC | NC |
| | HIST1H1E | Histone cluster 1 H1e | Nucleus | -0.57 | NC | -1.11 | NC | NC |

^aFC, fold change.

^bNC, no change. This refers to genes that exhibited no statistically significant change in expression between cells expressing a given GFP-Ank13 protein versus GFP or infected cells versus uninfected cells.

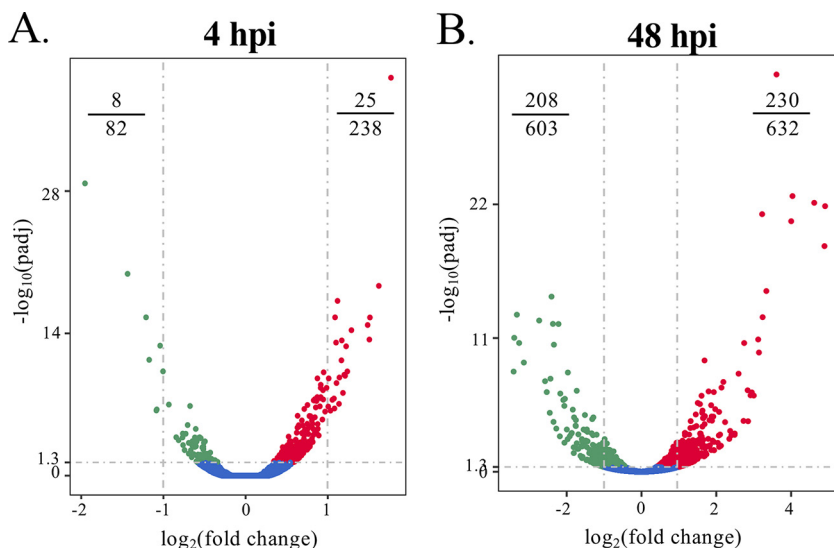


FIG 11 Differential gene expression profiles influenced by *O. tsutsugamushi* infection. Volcano plots showing differential expression profiles for cells infected with *O. tsutsugamushi* for 4 h (A) or 48 h (B) compared to uninfected cells. Gray horizontal dashed line indicates the threshold for significantly differentially expressed genes ($P_{adj} < 0.05$). Vertical dashes indicate genes exhibiting a $\log_2(\text{fold change})$ of >1 or <-1 . Each dot corresponds to an individual gene. Blue dots indicate no significant difference in infected cells compared to uninfected cells. Red and green dots indicate genes that are up- or downregulated, respectively, in cells expressing GFP fusions versus cells expressing GFP. Fractions in top corners denote the number of genes with $\log_2(\text{fold change})$ of >1 or <-1 out of the total number of differentially expressed genes.

second such residue in another, often adjacent AR that is contributory but not essential (57). Consistent with this trend, Ank13 I127 of AR4 is indispensable for and I161 of AR5 minorly aids the effector’s nucleotropism. Other nucleomodulins potentially exploit RaDAR. Anka, a nucleomodulin of the *Rickettsiales* pathogen *Anaplasma phagocytophilum* has conspicuous hydrophobic residues at the thirteenth position of consecutive ARs (61). *O. tsutsugamushi* Ank1 and Ank6 are putative nucleomodulins because they inhibit NF- κ B nuclear accumulation and its ability to activate transcription of a fluorescence reporter but have yet to be shown to directly alter expression of host genes. Ank1 and Ank6 utilize the importin α/β 1-dependent canonical nuclear localization route (16). Therefore, different *O. tsutsugamushi* effectors coopt two distinct eukaryotic nuclear import pathways. Functional diversification of *O. tsutsugamushi* Anks is also reflected in their spatiotemporal expression. Ank13 is most abundantly expressed and detectable in the nucleus during bacterial log-phase growth when risk for pathogen recognition by the host cell is highest. This period coincides with when the effector’s role in transcriptionally countering antimicrobial and other responses would be most needed. In contrast, expression of *ank4*, which contributes to invoking ER stress, coincides with induction of the unfolded protein response that provides amino acids to fuel *O. tsutsugamushi* growth (46).

Ank13 is predominantly a negative regulator of host cell gene expression. Its ability to alter host transcription involves its nucleotropism and interaction with the SCF ubiquitin ligase complex in both synergistic and mutually exclusive manners. Ank13_{I127R} which is incapable of nuclear translocation but retains the F-box, dysregulates expression of ~ 10 -fold fewer genes than nucleotropic Ank13 and Ank13 Δ F-box. Thus, Ank13 primarily targets host cell transcription within the nucleus but also does so in the cytoplasm conceivably by interacting with host cell transcription factors via its AR domain and promoting their polyubiquitination and proteasomal degradation in an F-box-dependent fashion. This phenomenon is reflected by the presence of *O. tsutsugamushi* Ank13 and GFP-Ank13 in both the nucleus and cytoplasm. Histone modification is one of the most prominent processes targeted by bacterial effectors for epigenetic control

(62). Ank13 and Ank13 Δ F-box commonly target numerous biological processes with histone modification, histone methylation, and chromatin modification being key among them. This means that Ank13 acts in the nucleus by negatively regulating cohorts of genes involved in large scale chromosome remodeling, potentially enacting epigenetic reprogramming of the host transcriptome and does so in an F-box-independent fashion. Perhaps Ank13 accomplishes this task by binding directly to distinct chromosomal regions, as has been demonstrated for AnkA and nucleomodulins Ank200, TRP32, TRP47, and TRP120 of another *Rickettsiales* member, *Ehrlichia chaffeensis* (61, 63–68). Alternatively, Ank13 could interact with transcription factors to sterically hinder their access to DNA.

The ubiquitin-proteasome system regulates transcription via polyubiquitination that leads to removal of DNA-associated proteins (69, 70). Cul1, an Ank13 interacting partner and SCF component, is abundant in the nucleus and associates with 23% of all DNA-associated protein degradation sites (69). In addition to commandeering the SCF complex in the cytoplasm, Ank13 does so in the nucleus as its major means of modulating gene expression. Indeed, Ank13 downregulates the most host genes by functioning in the nucleus in an F-box-dependent manner, as GFP-Ank13 alters transcription of roughly 2,000 distinct genes relative to GFP-Ank13 Δ F-box. The importance of the F-box to the ability of Ank13 to globally modulate eukaryotic processes is underscored by the yeast toxicity screen. Whereas Ank13_{1127R} toxicity was reduced 10-fold versus Ank13, removing the F-box lowered Ank13 toxicity 1,000-fold to render it non-toxic. Hence, Ank13 toxicity is predominantly linked to F-box-dependent modulation—most likely ubiquitination/proteasomal degradation—of host nuclear and cytoplasmic proteins that are critical for yeast survival.

The two largest categories of biological processes that Ank13 upregulates are associated with RNA/mRNA catabolism and protein targeting to membranes, the ER in particular. The former could be due to a cellular response to the global transcriptional repression that the effector induces or could be an Ank13-induced response to promote degradation of microRNAs, which contribute to antimicrobial responses and are known targets of various pathogens (62). The increase in ER-targeting genes correlates with *O. tsutsugamushi* induction of ER stress, the unfolded protein response, and secretory pathway inhibition (27, 46).

Many of the genes that Ank13 most strongly dysregulates correlate with phenotypes observed for *O. tsutsugamushi*-infected cells. One of the largest cohorts of most strongly downregulated genes are those involved in the inflammatory response, especially NF- κ B. *O. tsutsugamushi* activates NF- κ B translocation into the nucleus during the initial hours of infection, but this is soon reversed and remains so throughout infection (16, 20, 21). Whereas Ank1 and Ank6 impair NF- κ B accumulation in the nucleus (16), Ank13 contributes to the repression of this pathway by transcriptionally downregulating NF- κ B and related genes in F-box-dependent manners in the nucleus and cytoplasm. In agreement with these data, NFKB1, NFKB2, and several other pathogen recognition-induced genes that are upregulated in *O. tsutsugamushi*-infected cells at 4 h are either downregulated or quiescent by 48 h, a time point that coincides with Ank13 expression. Moreover, nearly all of the genes that are most strongly downregulated by GFP-Ank13 are suppressed in infected cells.

In sum, our report identifies *O. tsutsugamushi* Ank13 as a novel nucleomodulin and the first such effector to coopt RaDAR for nuclear translocation. Ank13 is a multifaceted protein that functions in the nucleus and cytoplasm via F-box-dependent and -independent manners to globally reprogram host cell transcription. Its conservation among scrub typhus patient isolates suggests that it serves an important role in colonizing mammalian hosts. Given the similarities between gene expression profiles of cells infected with *O. tsutsugamushi* and ectopically expressing Ank13, we posit that the bacterium deploys Ank13 as a key part of a global reprogramming strategy that maintains the host cell environment as a permissive niche.

MATERIALS AND METHODS

Cultivation of cell lines and *O. tsutsugamushi* infections. Uninfected HeLa cells (CCL-2; American Type Culture Collection [ATCC], Manassas, VA) and HeLa cells infected with *O. tsutsugamushi* str. Ikeda (NC_010793.1) were maintained as previously described (16). To obtain *O. tsutsugamushi* for experimental use, infected ($\geq 90\%$) HeLa cells that had been inoculated 72 to 96 h prior were mechanically disrupted using glass beads, followed by differential centrifugation to recover host cell-free bacteria as described previously (16). Unless stated otherwise, synchronous infections were performed using an MOI of 10. Experiments were verified for achieving the targeted MOI by assessing duplicate coverslips using antiserum specific for TSA56 (27) and immunofluorescence microscopy as described below.

Analysis of *ank13* homologs. The National Center for Biotechnology Information (NCBI) Nucleotide Basic Local Alignment Search Tool (BLAST; www.blast.ncbi.nlm.nih.gov) was used to identify homologs of Ikeda str. *ank13* (OTT_RS04140) present in the genomes of other *O. tsutsugamushi* strains in GenBank. Homologs were identified in Kato (KATO_02023), UT76 (UT76HP_00714), UT176 (UT176_01464), and Wuj/2014 (F0363_02935). To identify homologs in isolates for which genomic information was unavailable, primers *ank13*-853F and *ank13*-1260R (see Table S2), which target nucleotides corresponding to Ikeda *ank13* 853 to 1260 and are identical among the Kato, UT76, UT176, and Wuj/2014 *ank13* homologs, were used to amplify DNA from strains FPW2016, TM2532, SV445, UT169, UT177, and UT559 (71). PCR was performed using MyTaq DNA polymerase (Bioline, Taunton, MA). After an initial denaturing step at 95°C for 1 min, thermal cycling conditions were 35 cycles of 95°C for 15 s, 55°C for 15 s, and 72°C for 10 s, followed by a final extension at 72°C for 30 s. Amplicons were analyzed with 2.0% agarose gels in 40 mM Tris-acetate–2 mM EDTA (pH 8). To ensure the integrity of the template DNA and appropriate thermal cycling conditions, reactions were simultaneously conducted using primers that target the conserved eubacterial 16S rRNA sequence (71). Bands were excised and purified using the QIAquickGel Extraction kit (Qiagen, Germantown, MD). Isolated DNA was submitted for Sanger sequencing using *ank13*-853F and *ank13*-1260R primers (Genewiz, South Plainfield, NJ). The resulting sequences were aligned and analyzed using MegAlign, part of the Lasergene 15.3 software package (DNASTAR, Madison, WI). New partial coding sequences for *ank13* homologs have been deposited in GenBank for FPW2016 (MZ338370), TM2532 (MZ338375), SV445 (MZ338374), UT169 (MZ338371), UT177 (MZ338372), and UT559 (MZ338373).

Plasmid constructs. pFlag-Ank13 and pGFP-Ank13 were generated previously (29). Constructs encoding N-terminally Flag- and/or GFP-tagged Ank13₄₉₋₄₉₀, Ank13 Δ F-box, Ank13_{V62R}, Ank13_{A95R}, Ank13_{I127R}, Ank13_{I127L}, Ank13_{I161R}, and Ank13_{I161L} were generated using the TaKaRa Bio USA (San Francisco, CA) In-Fusion Mutagenesis protocol and pFlag-Ank13 or pGFP-Ank13 as the template. Primers used to introduce mutations (see Table S2) were designed using the In-Fusion Cloning Primer Design Tool v1.0 (TaKaRa Bio). pFlag-Ank13_{I127R/I161R} was made according to the same protocol and using pFlag-Ank13_{I127R} as the template. pGFP-Ank13 Δ F-box was constructed by digesting pFlag-Ank13 Δ F-box with EcoRI and BamHI and subcloning the released restriction fragment encoding Ank13 Δ F-box into the multicloning site of pEGFP-C1 (29). All plasmid constructs were confirmed by sequence analysis (Genewiz). pFlag-BAP (Sigma-Aldrich, St. Louis, MO), pFlag-Ank6 (29), pFlag-Ank9 (29), and empty pEGFP-C1 (29) were included as controls for experiments involving Flag- or GFP-tagged Ank13.

Ank13 antiserum generation. NCBI Protein BLAST (www.blast.ncbi.nlm.nih.gov) was used to confirm that Ank13 (WP_012461452.1) residues 288 to 360, encoded by *ank13* nucleotides 862 to 1080, are unique within the annotated *O. tsutsugamushi* Ikeda str. proteome. An *Escherichia coli* codon-optimized DNA sequence consisting of two tryptophan codons, followed by two successive repeats of *ank13* nucleotides 862 to 1080, was synthesized and cloned into pET-45b(+) downstream and in-frame with a 6 \times His tag coding sequence by GenScript (Piscataway, NJ). The two tryptophans were included to facilitate accurate protein concentration determination. The resulting construct was propagated in *E. coli* Stellar Competent Cells (TaKaRa Bio), miniprep, and transformed into *E. coli* BL21(DE3) cells (MilliporeSigma, Burlington, MA). After induction with 1 mM IPTG (isopropyl- β -D-thiogalactopyranoside), *E. coli* was lysed and the 6 \times His-tagged chimeric Ank13₂₈₈₋₃₆₀-Ank13₂₈₈₋₃₆₀ protein was purified from the insoluble phase as described previously (72). Briefly, cAnk13 was purified under nondenaturing conditions via gravity flow utilizing nickel-charged Poly-Prep Chromatography Columns (Bio-Rad, Hercules, CA) and 8 M urea buffer, followed by determination of protein concentration using a bicinchoninic acid assay (Thermo Fisher Scientific, Waltham, MA). An 8-week-old female Sprague-Dawley rat was immunized with 50 μ g of cAnk13 emulsified in a 1:1 ratio with complete Freund adjuvant and administered in a total volume of 400 μ l. At weeks 3 and 5, the rat was boosted with 25 μ g of protein in incomplete Freund adjuvant. At week 6, the rat was euthanized by CO₂ asphyxiation, blood was collected by cardiac puncture, and the Ank13 antiserum recovered. All animal research was performed under the approval of the Institutional Animal Care and Use Committee at Virginia Commonwealth University (protocol AD10000387).

Transfection. HeLa cells grown to approximately 90% confluence were transfected with plasmid DNA using Lipofectamine 2000 (Invitrogen, Carlsbad, CA) and incubated at 37°C in a humidified incubator at 5% atmospheric CO₂ for 18 to 24 h. The amount of plasmid DNA used for transfections was modified from that recommended by the Lipofectamine 2000 protocol (Invitrogen) per plasmid to accommodate various levels of transfection efficiency, as determined by enumerating Flag immunosignal-positive cells in indirect immunofluorescence assays or according to Western blot densitometric signal. Spent medium was removed. The cells were washed once with phosphate-buffered saline (PBS; 1.05 mM KH₂PO₄, 155 mM NaCl, 2.96 mM Na₂HPO₄ [pH 7.4]) before being processed for immunofluorescence microscopy, Western blotting, immunoprecipitation, or cell sorting.

Immunofluorescence microscopy. HeLa cells were seeded onto glass coverslips within 24-well plates and transfected to express Flag-tagged protein for 18 h. To inhibit nuclear import, 3 h prior to collection (16 h posttransfection), spent medium was replaced with fresh media containing either 50 μ M importazole (Sigma-Aldrich) or dimethyl sulfoxide (DMSO) as a vehicle control prior to fixation. Fixed cells were washed with PBS prior to fixation and permeabilization with -20°C methanol. Coverslips were blocked in 5% (vol/vol) bovine serum albumin (BSA) in PBS. Coverslips were then incubated with rabbit or mouse anti-Flag (Sigma-Aldrich [F1804], 1:1,000) or rat anti-Ank13 (1:1,000), followed by incubation with Alexa Fluor 488-conjugated goat anti-rabbit or -mouse and/or Alexa Fluor 594-conjugated goat anti-rat (Invitrogen, 1:1,000) in 5% BSA. Blocking and antibody incubations were performed for 1 h at room temperature with three PBS washes between each step. Samples were incubated with 0.1 μ g ml^{-1} DAPI (4',6'-diamidino-2-phenylindole; Invitrogen) in PBS for 1 min, washed three times with PBS, and mounted with ProLong Gold Antifade mounting media (Invitrogen). Coverslips were imaged with an Olympus BX51 spinning disc confocal microscope (Olympus, Shinjuku City, Tokyo, Japan). Cells were scored for immunosignal subcellular localization by counting 100 cells per coverslip.

Western blotting. For infection studies using whole-cell lysates, cells were washed with PBS, harvested, centrifuged at $10,000 \times g$ for 10 min, and lysed in radioimmunoprecipitation assay buffer (50 mM Tris-HCl [pH 7.4], 150 mM NaCl, 1% NP-40, 1% sodium deoxycholate, 1 mM EDTA [pH 8]) containing Halt protease and phosphatase inhibitor cocktail (Thermo Fisher Scientific). Protein lysate concentrations were determined using a Bradford assay (Bio-Rad). Equivalent amounts of lysates were resolved by SDS-PAGE in 4 to 15% TGX polyacrylamide gels (Bio-Rad) at 110 V for 15 min, followed by 200 V for 25 min. Proteins were transferred onto nitrocellulose membrane in Towbin buffer at 100 V for 30 min. Blots were blocked and probed with either 5% (vol/vol) nonfat dry milk or 5% (vol/vol) BSA in Tris-buffered saline plus 0.05% Tween 20 (TBS-T) and then were screened with rabbit or mouse anti-Flag (Sigma-Aldrich [catalog number F7425 or F1804], 1:1,000), rabbit anti-lamin A/C (Cell Signaling, Danvers, MA [20325]; 1:1,000), mouse anti-GAPDH (Santa Cruz, Dallas, TX [sc-365062]; 1:750), rat anti-Ank13 at 1:1,000, rabbit anti-TSA56 (27; 1:1,000), rat anti-NLRC5 (MilliporeSigma [MABF260]; 1:1000), rabbit anti-Cul1 (Abcam, Cambridge, United Kingdom [ab75817]; 1:1,000), rabbit anti-Skp1 (Cell Signaling [21565]; 1:750), and rabbit anti-Rbx1 (Abcam [ab133565]; 1:1,000). Bound primary antibodies were detected using horseradish peroxidase-conjugated horse anti-mouse, anti-rabbit, or anti-rat IgG (Cell Signaling Technology; 1:10,000). All blots were incubated with either SuperSignal West Pico PLUS, SuperSignal West Dura, or SuperSignal West Femto chemiluminescent substrate (Thermo Fisher Scientific) prior to imaging in a ChemiDoc Touch Imaging System (Bio-Rad). Bio-Rad Image Lab 6.0 software was used to obtain densitometric values.

Cytoplasmic and nuclear fractionation. Transfected or *O. tsutsugamushi*-infected HeLa cells were washed with PBS, harvested, and lysed following the nuclear fractionation kit (Abcam) protocol. In a singular case when it was necessary to increase endogenous NLRC5 levels prior to fractionation, HeLa cells were stimulated with 20 ng ml^{-1} human IFN- γ (PeproTech, Rock Hill, NJ) for 18 h. To inhibit nuclear import, 3 h prior to collection (16 h posttransfection), spent medium was replaced with fresh media containing either 50 μ M importazole (Sigma-Aldrich) or DMSO as a vehicle control prior to nuclear fractionation. Cytoplasmic and nuclear fraction lysates were resolved by SDS-PAGE and subjected to Western blot analysis.

Immunoprecipitation. Transfected HeLa cells were harvested and lysed in high saline Tris buffer (50 mM Tris HCl, 400 mM NaCl, 1 mM EDTA [pH 7.4]) with 1.0% Triton x-100 (TBHS-T) spiked with Halt protease and phosphatase inhibitor cocktail (Thermo Fisher Scientific). Protein A/G agarose beads (Thermo Fisher Scientific) were washed with TBHS-T buffer three times, centrifuged at $8,400 \times g$ for 30 s, and added to normalized cell lysates in a final volume of 400 μ l. The samples were rotated with beads at 4°C for 4 h, followed by centrifugation at $8,600 \times g$ for 30 s. Recovered supernatants were added to Anti-Flag M2 affinity gel (MilliporeSigma) that had been washed with TBHS-T buffer three times. Samples were rotated with beads at 4°C overnight followed by centrifugation at $8,600 \times g$ for 30 s and washing with TBHS-T 6 to 10 times. Washed beads were resuspended in Laemmli buffer and incubated at 100°C for 5 min to elute bound proteins. Inputs (30 μ g) and eluates were resolved by SDS-PAGE and screened by Western blotting.

RNA isolation and RT-qPCR. Total RNA was isolated from synchronously infected cells at 2, 4, 8, 24, 48, and 72 h using the RNeasy minikit (Qiagen). Then, 1 μ g RNA was treated with amplification-grade DNase (Invitrogen). cDNA was generated using the iScript reverse transcription supermix protocol (Bio-Rad). To verify successful genomic DNA depletion, parallel reactions performed in the absence of reverse transcriptase were used as the template for PCR with human *GAPDH*-specific primers (19) and MyTaq polymerase (Bioline, Taunton, MA) as described above. qPCR using cDNA as the template was performed with SsoFast EvaGreen supermix (Bio-Rad) and *GAPDH*, *O. tsutsugamushi* 16S rDNA (*ott16S*) (29), and *ank13* primers (29). Thermal cycling conditions used were 95°C for 30 s, followed by 40 cycles of 95°C for 5 s and 55°C for 5 s. Relative expression was determined using the $2^{-\Delta\Delta\text{CT}}$ method (73) as part of the CFX Maestro for Mac 1.0 software package (Bio-Rad).

Yeast toxicity assays. Inserts encoding Ank13, Ank13_{1127R}, and Ank13 Δ F-box were cloned into a modified pYesNTA-Kan vector (74) to be in-frame with both the Gal promoter and His-tag. The *ank13* coding sequence was PCR amplified using primers *ank13*+1 KpnI F and *ank13* XbaI R (see Table S2), Platinum *Taq* DNA polymerase High Fidelity (Invitrogen), and pFlag-Ank13 as the template. Thermal cycling conditions were 98°C for 30 s, followed by 25 cycles of 98°C for 10 s, 55°C for 30 s, and 72°C for 2 min, and a final extension at 72°C for 10 min. *ank13* Δ F-box was PCR amplified using primers *ank13*+1 KpnI F and *ank13* Δ F-box XbaI R (see Table S2), Platinum *Taq* DNA polymerase High Fidelity, and pFlag-Ank13 Δ F-box as the template. Amplicons were digested with KpnI-HF and XbaI, gel purified, and ligated into pYesNTA-Kan to generate pYes-Ank13 and pYes-Ank13 Δ F-box. pYes-Ank13_{1127R} was engineered using pYes-Ank13 as the template, In-Fusion primers Ank13_{1127R} F and Ank13_{1127R} R (see Table S2) according to the TaKaRa Bio USA In-Fusion mutagenesis protocol. Construct sequence integrity was verified by

DNA sequencing (Genewiz). The toxicity of Ank13, Ank13_{1127R} and Ank13ΔF-box in *S. cerevisiae* W303 was assessed as described previously (74). Briefly, *S. cerevisiae* was transformed with pYesNTA-Kan constructs for expressing Ank13, Ank13_{1127R}, Ank13ΔF-box, *C. trachomatis* CT694 (75), or empty pYesNTA-Kan. Yeast transformants were plated on uracil dropout media containing glucose. Individual colonies were selected and expanded in uracil dropout broth containing glucose. Toxicity was assessed by dilution to an optical density at 600 nm of 0.2 and spotting 10-fold serial dilutions onto 2% glucose (noninducing conditions) and 2% galactose (inducing expression of the fusion protein) agar plates and incubated at 30°C for 48 h. Images were captured using a UVP GelDoc-It (Analytik Jena, Jena, Germany).

RNA-seq. HeLa cells transfected to express GFP-Ank13, -Ank13_{1127R}, -Ank13ΔF-box, or GFP were washed with PBS, trypsinized, and recovered by centrifugation at 500 × *g* for 5 min. The resulting cell pellets were resuspended in 1 ml of filtered EDTA (Versene) solution (0.526 mM; Irvine Scientific, Santa Ana, CA) with 2% (vol/vol) heat-inactivated fetal bovine serum (FBS). GFP-expressing cells were sorted from nontransfected cells on a FACSAria Fusion SORP High-Speed Cell Sorter using BD FACSDiva 8.0.1 (BD Biosciences) and collected in 10% (vol/vol) FBS in PBS. Histograms of transfected and nontransfected control cells were generated using FloJo V10 software (BD Biosciences). Total RNA isolated from triplicate samples of each sorted population and HeLa cells that had been synchronously infected with *O. tsutsugamushi* for 4 h or 48 h were submitted to Novogene (Sacramento, CA) for RNA-seq analyses as follows. Sample integrity was confirmed using an Agilent 2100 Bioanalyzer (Agilent Technologies, Santa Clara, CA). Reads were mapped to human reference genome (GRCh38/hg38) sequenced to a paired-end 250- to 300-bp insert cDNA library using an Illumina high-throughput sequencing platform (Illumina, San Diego, CA). Alignments were parsed using STAR program. Venn diagram and volcano plot analyses were achieved through differential expression significant analysis of two conditions or groups using the DESeq2 R software package 1.14.1 (Bioconductor). Resulting *P* values were adjusted using Benjamini and Hochberg's approach for controlling the false discovery rate (76). The differential expression criterion was an adjusted *P* value (P_{adj}) < 0.05 and based on the negative binomial distribution (58). Genes were classified per biological processes by analyzing Gene Ontology (GO) terms (www.geneontology.org). The R package, ClusterProfiler (77), was used for statistical analysis of GO and those terms with a corrected *P* value of <0.05 were considered significantly enriched.

Bioinformatic analysis. cNLS Mapper (http://nls-mapper.iab.keio.ac.jp/cgi-bin/NLS_Mapper_form.cgi) (52) was used to predict importin α -dependent nuclear localization signals. STRING (59) was used to analyze protein-protein interaction networks (<https://string-db.org/cgi/input.pl>).

Statistical analysis. Statistical analyses were performed using the Prism 8.0 software package (GraphPad, San Diego, CA). One-way analysis of variance (ANOVA) with Tukey's *post hoc* test was used to test for a significant difference among groups. Two-way ANOVA with Dunnett's correction was used to assess for significant differences among the percentages of cells exhibiting cytoplasmic, throughout the cell, or nuclear localization of Flag-tagged proteins. Statistical significance was set at *P* values of <0.05.

SUPPLEMENTAL MATERIAL

Supplemental material is available online only.

TABLE S1, DOCX file, 0.01 MB.

TABLE S2, DOCX file, 0.02 MB.

DATA SET S1, XLSX file, 1 MB.

DATA SET S2, XLSX file, 0.6 MB.

DATA SET S3, XLSX file, 0.8 MB.

FIG S1, TIFF file, 3.1 MB.

FIG S2, TIFF file, 1.5 MB.

FIG S3, TIFF file, 0.1 MB.

FIG S4, TIFF file, 0.8 MB.

FIG S5, TIFF file, 3.6 MB.

ACKNOWLEDGMENTS

We thank Travis Folley for analytical assistance.

This study was supported by National Institutes of Health/National Institute of Allergy and Infectious Diseases) grants R01 AI123346 and R21 AI152513 to J.A.C., R01 AI150812 and R01 AI155434 to M.M.W., and R01 AI14180 to R.T.M. and by a American Heart Association grant 20PRE35210610 to H.E.A. Cell sorting was performed by the VCU Massey Cancer Center Flow Cytometry Shared Resource, supported, in part, with funding from NIH-NCI Cancer Center Support Grant P30 CA016059.

REFERENCES

1. Biernie H, Pourpre R. 2020. Bacterial factors targeting the nucleus: the growing family of nucleomodulins. *Toxins* 12:220. <https://doi.org/10.3390/toxins12040220>.
2. Hanford HE, Von Dwingelo J, Abu Kwaiq Y. 2021. Bacterial nucleomodulins: a coevolutionary adaptation to the eukaryotic command center. *PLoS Pathog* 17:e1009184. <https://doi.org/10.1371/journal.ppat.1009184>.

3. Luce-Fedrow A, Lehman ML, Kelly DJ, Mullins K, Maina AN, Stewart RL, Ge H, John HS, Jiang J, Richards AL. 2018. A review of scrub typhus (*Orientia tsutsugamushi* and related organisms): then, now, and tomorrow. *Tropical Med* 3:8. <https://doi.org/10.3390/tropicalmed3010008>.
4. Xu G, Walker DH, Jupiter D, Melby PC, Arcari CM. 2017. A review of the global epidemiology of scrub typhus. *PLoS Negl Trop Dis* 11:e0006062. <https://doi.org/10.1371/journal.pntd.0006062>.
5. Weitzel T, Martínez-Valdebenito C, Acosta-Jamett G, Jiang J, Richards AL, Abarca K. 2019. Scrub typhus in continental Chile, 2016–2018. *Emerg Infect Dis* 25:1214–1217. <https://doi.org/10.3201/eid2506.181860>.
6. Weitzel T, Dittrich S, López J, Phuklia W, Martínez-Valdebenito C, Velásquez K, Blacksell SD, Paris DH, Abarca K. 2016. Endemic scrub typhus in South America. *N Engl J Med* 375:954–961. <https://doi.org/10.1056/NEJMoa1603657>.
7. Izzard L, Fuller A, Blacksell SD, Paris DH, Richards AL, Aukkanit N, Nguyen C, Jiang J, Fenwick S, Day NP, Graves S, Stenos J. 2010. Isolation of a novel *Orientia* species (*O. chuto* sp. nov.) from a patient infected in Dubai. *J Clin Microbiol* 48:4404–4409. <https://doi.org/10.1128/JCM.01526-10>.
8. Abarca K, Martínez-Valdebenito C, Angulo J, Jiang J, Farris CM, Richards AL, Acosta-Jamett G, Weitzel T. 2020. Molecular description of a novel *Orientia* species causing scrub typhus in Chile. *Emerg Infect Dis* 26:2148–2156. <https://doi.org/10.3201/eid2609.200918>.
9. Paris DH, Phetsouvanh R, Tanganuchitcharnchai A, Jones M, Jenjaroen K, Vongsouvath M, Ferguson DP, Blacksell SD, Newton PN, Day NP, Turner GD. 2012. *Orientia tsutsugamushi* in human scrub typhus eschars shows tropism for dendritic cells and monocytes rather than endothelium. *PLoS Negl Trop Dis* 6:e1466. <https://doi.org/10.1371/journal.pntd.0001466>.
10. Tantibhedhyangkul W, Prachason T, Waywa D, El Filali A, Ghigo E, Thongnoppakhun W, Raoult D, Suputtamongkol Y, Capo C, Limwongse C, Mege J-L. 2011. *Orientia tsutsugamushi* stimulates an original gene expression program in monocytes: relationship with gene expression in patients with scrub typhus. *PLoS Negl Trop Dis* 5:e1028. <https://doi.org/10.1371/journal.pntd.0001028>.
11. Mika-Gospodorz B, Giengkam S, Westermann AJ, Wongsantichon J, Kion-Crosby W, Chuenklin S, Wang LC, Sunyakumthorn P, Sobota RM, Subbian S, Vogel J, Barquist L, Salje J. 2020. Dual RNA-seq of *Orientia tsutsugamushi* informs on host-pathogen interactions for this neglected intracellular human pathogen. *Nat Commun* 11:3363. <https://doi.org/10.1038/s41467-020-17094-8>.
12. Soong L, Wang H, Shelite TR, Liang Y, Mendell NL, Sun J, Gong B, Valbuena GA, Bouyer DH, Walker DH. 2014. Strong type 1, but impaired type 2, immune responses contribute to *Orientia tsutsugamushi*-induced pathology in mice. *PLoS Negl Trop Dis* 8:e3191. <https://doi.org/10.1371/journal.pntd.0003191>.
13. Tantibhedhyangkul W, Ben Amara A, Textoris J, Gorvel L, Ghigo E, Capo C, Mege JL. 2013. *Orientia tsutsugamushi*, the causative agent of scrub typhus, induces an inflammatory program in human macrophages. *Microb Pathog* 55:55–63. <https://doi.org/10.1016/j.micpath.2012.10.001>.
14. Xu G, Mendell NL, Liang Y, Shelite TR, Goez-Rivillas Y, Soong L, Bouyer DH, Walker DH. 2017. CD8⁺ T cells provide immune protection against murine disseminated endotheliotropic *Orientia tsutsugamushi* infection. *PLoS Negl Trop Dis* 11:e0005763. <https://doi.org/10.1371/journal.pntd.0005763>.
15. Shelite TR, Liang Y, Wang H, Mendell NL, Trent BJ, Sun J, Gong B, Xu G, Hu H, Bouyer DH, Soong L. 2016. IL-33-dependent endothelial activation contributes to apoptosis and renal injury in *Orientia tsutsugamushi*-infected mice. *PLoS Negl Trop Dis* 10:e0004467. <https://doi.org/10.1371/journal.pntd.0004467>.
16. Evans SM, Rodino KG, Adcox HE, Carlyon JA. 2018. *Orientia tsutsugamushi* uses two Ank effectors to modulate NF- κ B p65 nuclear transport and inhibit NF- κ B transcriptional activation. *PLoS Pathog* 14:e1007023. <https://doi.org/10.1371/journal.ppat.1007023>.
17. Kang SJ, Jin HM, Cho YN, Oh TH, Kim SE, Kim UJ, Park KH, Jang HC, Jung SI, Kee SJ, Park YW. 2018. Dysfunction of circulating natural killer T cells in patients with scrub typhus. *J Infect Dis* 218:1813–1821. <https://doi.org/10.1093/infdis/jiy402>.
18. Kim MK, Kang JS. 2001. *Orientia tsutsugamushi* suppresses the production of inflammatory cytokines induced by its own heat-stable component in murine macrophages. *Microb Pathog* 31:145–150. <https://doi.org/10.1006/mpat.2001.0457>.
19. Rodino KG, Adcox HE, Martin RK, Patel V, Conrad DH, Carlyon JA. 2019. The obligate intracellular bacterium *Orientia tsutsugamushi* targets NLR5 to modulate the major histocompatibility complex class I pathway. *Infect Immun* 87:813–811. <https://doi.org/10.1128/IAI.00876-18>.
20. Cho NH, Seong SY, Huh MS, Kim NH, Choi MS, Kim IS. 2002. Induction of the gene encoding macrophage chemoattractant protein 1 by *Orientia tsutsugamushi* in human endothelial cells involves activation of transcription factor activator protein 1. *Infect Immun* 70:4841–4850. <https://doi.org/10.1128/IAI.70.9.4841-4850.2002>.
21. Cho NH, Seong SY, Huh MS, Han TH, Koh YS, Choi MS, Kim IS. 2000. Expression of chemokine genes in murine macrophages infected with *Orientia tsutsugamushi*. *Infect Immun* 68:594–602. <https://doi.org/10.1128/IAI.68.2.594-602.2000>.
22. Ko Y, Choi JH, Ha NY, Kim IS, Cho NH, Choi MS. 2013. Active escape of *Orientia tsutsugamushi* from cellular autophagy. *Infect Immun* 81:552–559. <https://doi.org/10.1128/IAI.00861-12>.
23. Choi JH, Cheong TC, Ha NY, Ko Y, Cho CH, Jeon JH, So I, Kim IK, Choi MS, Kim IS, Cho NH. 2013. *Orientia tsutsugamushi* subverts dendritic cell functions by escaping from autophagy and impairing their migration. *PLoS Negl Trop Dis* 7:e1981. <https://doi.org/10.1371/journal.pntd.0001981>.
24. Jernigan KK, Bordenstein SR. 2014. Ankyrin domains across the Tree of Life. *PeerJ* 2:e264. <https://doi.org/10.7717/peerj.264>.
25. Kane EI, Spratt DE. 2021. Structural insights into ankyrin repeat-containing proteins and their influence in ubiquitylation. *Int J Mol Sci* 22:609. <https://doi.org/10.3390/ijms22020609>.
26. Nakayama K, Yamashita A, Kurokawa K, Morimoto T, Ogawa M, Fukuhara M, Urakami H, Ohnishi M, Uchiyama I, Ogura Y, Ooka T, Oshima K, Tamura A, Hattori M, Hayashi T. 2008. The Whole-genome sequencing of the obligate intracellular bacterium *Orientia tsutsugamushi* revealed massive gene amplification during reductive genome evolution. *DNA Res* 15:185–199. <https://doi.org/10.1093/dnares/dsn011>.
27. Beyer AR, Rodino KG, VieBrock L, Green RS, Tegels BK, Oliver LD, Marconi RT, Carlyon JA. 2017. *Orientia tsutsugamushi* Ank9 is a multifunctional effector that utilizes a novel GRIP-like Golgi localization domain for Golgi-to-endoplasmic reticulum trafficking and interacts with host COPB2. *Cell Microbiol* 19:e12727. <https://doi.org/10.1111/cmi.12727>.
28. Min CK, Kwon YJ, Ha NY, Cho BA, Kim JM, Kwon EK, Kim YS, Choi MS, Kim IS, Cho NH. 2014. Multiple *Orientia tsutsugamushi* ankyrin repeat proteins interact with SCF1 ubiquitin ligase complex and eukaryotic elongation factor 1 α . *PLoS One* 9:e105652. <https://doi.org/10.1371/journal.pone.0105652>.
29. VieBrock L, Evans SM, Beyer AR, Larson CL, Beare PA, Ge H, Singh S, Rodino KG, Heinzen RA, Richards AL, Carlyon JA. 2014. *Orientia tsutsugamushi* ankyrin repeat-containing protein family members are type 1 secretion system substrates that traffic to the host cell endoplasmic reticulum. *Front Cell Infect Microbiol* 4:186. <https://doi.org/10.3389/fcimb.2014.00186>.
30. Beyer AR, VieBrock L, Rodino KG, Miller DP, Tegels BK, Marconi RT, Carlyon JA. 2015. *Orientia tsutsugamushi* strain Ikeda ankyrin repeat-containing proteins recruit SCF1 ubiquitin ligase machinery via poxvirus-like F-box motifs. *J Bacteriol* 197:3097–3109. <https://doi.org/10.1128/JB.00276-15>.
31. Nguyen KM, Busino L. 2020. The biology of F-box proteins: the SCF family of E3 ubiquitin ligases. *Adv Exp Med Biol* 1217:111–122. https://doi.org/10.1007/978-981-15-1025-0_8.
32. Price CT, Kwaik YA. 2010. Exploitation of host polyubiquitination machinery through molecular mimicry by eukaryotic-like bacterial F-box effectors. *Front Microbiol* 1:122. <https://doi.org/10.3389/fmicb.2010.00122>.
33. Price CT, Al-Khodor S, Al-Quadan T, Santic M, Habyarimana F, Kalia A, Kwaik YA. 2009. Molecular mimicry by an F-box effector of *Legionella pneumophila* hijacks a conserved polyubiquitination machinery within macrophages and protozoa. *PLoS Pathog* 5:e1000704. <https://doi.org/10.1371/journal.ppat.1000704>.
34. Lomma M, Dervins-Ravault D, Rolando M, Nora T, Newton HJ, Sansom FM, Sahr T, Gomez-Valero L, Jules M, Hartland EL, Buchrieser C. 2010. The *Legionella pneumophila* F-box protein Lpp2082 (AnkB) modulates ubiquitination of the host protein parvin B and promotes intracellular replication. *Cell Microbiol* 12:1272–1291. <https://doi.org/10.1111/j.1462-5822.2010.01467.x>.
35. Price CT, Al-Quadan T, Santic M, Rosenshine I, Abu Kwaik Y. 2011. Host proteasomal degradation generates amino acids essential for intracellular bacterial growth. *Science* 334:1553–1557. <https://doi.org/10.1126/science.1212868>.
36. Wong K, Perpich JD, Kozlov G, Cygler M, Abu Kwaik Y, Gehring K. 2017. Structural mimicry by a bacterial F box effector hijacks the host ubiquitin-proteasome system. *Structure* 25:376–383. <https://doi.org/10.1016/j.str.2016.12.015>.
37. Herbert MH, Squire CJ, Mercer AA. 2015. Poxviral ankyrin proteins. *Viruses* 7:709–738. <https://doi.org/10.3390/v7020709>.

38. Sonnberg S, Seet BT, Pawson T, Fleming SB, Mercer AA. 2008. Poxvirus ankyrin repeat proteins are a unique class of F-box proteins that associate with cellular SCF1 ubiquitin ligase complexes. *Proc Natl Acad Sci U S A* 105:10955–10960. <https://doi.org/10.1073/pnas.0802042105>.
39. Li T, Lu Q, Wang G, Xu H, Huang H, Cai T, Kan B, Ge J, Shao F. 2013. SET-domain bacterial effectors target heterochromatin protein 1 to activate host rDNA transcription. *EMBO Rep* 14:733–740. <https://doi.org/10.1038/embor.2013.86>.
40. Pennini ME, Perrinet S, Dautry-Varsat A, Subtil A. 2010. Histone methylation by NUE, a novel nuclear effector of the intracellular pathogen *Chlamydia trachomatis*. *PLoS Pathog* 6:e1000995. <https://doi.org/10.1371/journal.ppat.1000995>.
41. Tamura A, Takahashi K, Tsuruhara T, Urakami H, Miyamura S, Sekikawa H, Kenmotsu M, Shibata M, Abe S, Nezu H. 1984. Isolation of *Rickettsia tsutsugamushi* antigenically different from Kato, Karp, and Gilliam strains from patients. *Microbiol Immunol* 28:873–882. <https://doi.org/10.1111/j.1348-0421.1984.tb00743.x>.
42. Shishido A, Ohtawara M, Tateno S, Mizuno S, Ogura M, Kitaoka M. 1958. The nature of immunity against scrub typhus in mice. I. The resistance of mice, surviving subcutaneous infection of scrub typhus rickettsia, to intraperitoneal reinfection of the same agent. *Jap J M Sci Biol* 11:383–399. <https://doi.org/10.7883/yoken1952.11.383>.
43. Luksameetanasan R, Blacksell SD, Kalambaheti T, Wuthiekanun V, Chierakul W, Chueasuwanchai S, Apiwattanaporn A, Stenos J, Graves S, Peacock SJ, Day NP. 2007. Patient and sample-related factors that effect the success of *in vitro* isolation of *Orientia tsutsugamushi*. *Southeast Asian J Trop Med Public Health* 38:91–96.
44. Paris DH, Aukkanit N, Jenjaroen K, Blacksell SD, Day NP. 2009. A highly sensitive quantitative real-time PCR assay based on the *groEL* gene of contemporary Thai strains of *Orientia tsutsugamushi*. *Clin Microbiol Infect* 15:488–495. <https://doi.org/10.1111/j.1469-0691.2008.02671.x>.
45. Phetsouvanh R, Sonthayanon P, Pukrittayakamee S, Paris DH, Newton PN, Feil EJ, Day NP. 2015. The diversity and geographical structure of *Orientia tsutsugamushi* strains from scrub typhus patients in Laos. *PLoS Negl Trop Dis* 9:e0004024. <https://doi.org/10.1371/journal.pntd.0004024>.
46. Rodino KG, VieBrock L, Evans SM, Ge H, Richards AL, Carlyon JA. 2018. *Orientia tsutsugamushi* modulates endoplasmic reticulum-associated degradation to benefit its growth. *Infect Immun* 86:e00596–17. <https://doi.org/10.1128/IAI.00596-17>.
47. Giengkam S, Blakes A, Utsahajit P, Chaemchuen S, Atwal S, Blacksell SD, Paris DH, Day NPJ, Salje J. 2015. Improved quantification, propagation, purification and storage of the obligate intracellular human pathogen *Orientia tsutsugamushi*. *PLoS Negl Trop Dis* 9:e0004009. <https://doi.org/10.1371/journal.pntd.0004009>.
48. Ko Y, Cho NH, Cho BA, Kim IS, Choi MS. 2011. Involvement of Ca²⁺ signaling in intracellular invasion of nonphagocytic host cells by *Orientia tsutsugamushi*. *Microb Pathog* 50:326–330. <https://doi.org/10.1016/j.micpath.2011.02.007>.
49. Ha NY, Cho NH, Kim YS, Choi MS, Kim IS. 2011. An autotransporter protein from *Orientia tsutsugamushi* mediates adherence to nonphagocytic host cells. *Infect Immun* 79:1718–1727. <https://doi.org/10.1128/IAI.01239-10>.
50. Chen HW, Zhang Z, Huber E, Mutumanje E, Chao CC, Ching WM. 2011. Kinetics and magnitude of antibody responses against the conserved 47-kilodalton antigen and the variable 56-kilodalton antigen in scrub typhus patients. *Clin Vaccine Immunol* 18:1021–1027. <https://doi.org/10.1128/CVI.00017-11>.
51. Urakami H, Tsuruhara T, Tamura A. 1982. Intranuclear *Rickettsia tsutsugamushi* in cultured mouse fibroblasts (L cells). *Microbiol Immunol* 26:445–447. <https://doi.org/10.1111/j.1348-0421.1982.tb00196.x>.
52. Kosugi S, Hasebe M, Tomita M, Yanagawa H. 2009. Systematic identification of cell cycle-dependent yeast nucleocytoplasmic shuttling proteins by prediction of composite motifs. *Proc Natl Acad Sci U S A* 106:10171–10176. <https://doi.org/10.1073/pnas.0900604106>.
53. Stewart M. 2007. Molecular mechanism of the nuclear protein import cycle. *Nat Rev Mol Cell Biol* 8:195–208. <https://doi.org/10.1038/nrm2114>.
54. Tripp KW, Barrick D. 2004. The tolerance of a modular protein to duplication and deletion of internal repeats. *J Mol Biol* 344:169–178. <https://doi.org/10.1016/j.jmb.2004.09.038>.
55. Soderholm JF, Bird SL, Kalab P, Sampathkumar Y, Hasegawa K, Uehara-Bingen M, Weis K, Heald R. 2011. Importazole, a small molecule inhibitor of the transport receptor importin-beta. *ACS Chem Biol* 6:700–708. <https://doi.org/10.1021/cb2000296>.
56. Meissner TB, Li A, Biswas A, Lee K-H, Liu Y-J, Bayir E, Iliopoulos D, van den Elsen PJ, Kobayashi KS. 2010. NLR family member NLRC5 is a transcriptional regulator of MHC class I genes. *Proc Natl Acad Sci U S A* 107:13794–13799. <https://doi.org/10.1073/pnas.1008684107>.
57. Lu M, Zak J, Chen S, Sanchez-Pulido L, Severson DT, Endicott J, Ponting CP, Schofield CJ, Lu X. 2014. A code for RanGDP binding in ankyrin repeats defines a nuclear import pathway. *Cell* 157:1130–1145. <https://doi.org/10.1016/j.cell.2014.05.006>.
58. Anders S, Huber W. 2010. Differential expression analysis for sequence count data. *Genome Biol* 11:R106. <https://doi.org/10.1186/gb-2010-11-10-r106>.
59. Szklarczyk D, Gable AL, Lyon D, Junge A, Wyder S, Huerta-Cepas J, Simonovic M, Doncheva NT, Morris JH, Bork P, Jensen LJ, Mering CV. 2019. STRING v11: protein-protein association networks with increased coverage, supporting functional discovery in genome-wide experimental datasets. *Nucleic Acids Res* 47:D607–D613. <https://doi.org/10.1093/nar/gky1131>.
60. Cornejo E, Schlaermann P, Mukherjee S. 2017. How to rewire the host cell: a home improvement guide for intracellular bacteria. *J Cell Biol* 216:3931–3948. <https://doi.org/10.1083/jcb.201701095>.
61. Rennoll-Bankert KE, Garcia-Garcia JC, Sinclair SH, Dumler JS. 2015. Chromatin-bound bacterial effector ankyrin A recruits histone deacetylase 1 and modifies host gene expression. *Cell Microbiol* 17:1640–1652. <https://doi.org/10.1111/cmi.12461>.
62. Denzer L, Schroten H, Schwerk C. 2020. From gene to protein: how bacterial virulence factors manipulate host gene expression during infection. *Int J Mol Sci* 21:3730. <https://doi.org/10.3390/ijms21103730>.
63. Wakeel A, den Dulk-Ras A, Hooykaas PJ, McBride JW. 2011. *Ehrlichia chaffeensis* tandem repeat proteins and Ank200 are type 1 secretion system substrates related to the repeats-in-toxin exoprotein family. *Front Cell Infect Microbiol* 1:22. <https://doi.org/10.3389/fcimb.2011.00022>.
64. Zhu B, Kuriakose JA, Luo T, Ballesteros E, Gupta S, Fofanov Y, McBride JW. 2011. *Ehrlichia chaffeensis* TRP120 binds a G+C-rich motif in host cell DNA and exhibits eukaryotic transcriptional activator function. *Infect Immun* 79:4370–4381. <https://doi.org/10.1128/IAI.05422-11>.
65. Luo T, Kuriakose JA, Zhu B, Wakeel A, McBride JW. 2011. *Ehrlichia chaffeensis* TRP120 interacts with a diverse array of eukaryotic proteins involved in transcription, signaling, and cytoskeleton organization. *Infect Immun* 79:4382–4391. <https://doi.org/10.1128/IAI.05608-11>.
66. Luo T, McBride JW. 2012. *Ehrlichia chaffeensis* TRP32 interacts with host cell targets that influence intracellular survival. *Infect Immun* 80:2297–2306. <https://doi.org/10.1128/IAI.00154-12>.
67. Farris TR, Dunphy PS, Zhu B, Kibler CE, McBride JW. 2016. *Ehrlichia chaffeensis* TRP32 is a nucleomodulin that directly regulates expression of host genes governing differentiation and proliferation. *Infect Immun* 84:3182–3194. <https://doi.org/10.1128/IAI.00657-16>.
68. Kibler CE, Milligan SL, Farris TR, Zhu B, Mitra S, McBride JW. 2018. *Ehrlichia chaffeensis* TRP47 enters the nucleus via a MYND-binding domain-dependent mechanism and predominantly binds enhancers of host genes associated with signal transduction, cytoskeletal organization, and immune response. *PLoS One* 13:e0205983. <https://doi.org/10.1371/journal.pone.0205983>.
69. Sweeney MA, Iakova P, Maneix L, Shih FY, Cho HE, Sahin E, Catic A. 2020. The ubiquitin ligase Cullin-1 associates with chromatin and regulates transcription of specific c-MYC target genes. *Sci Rep* 10:13942. <https://doi.org/10.1038/s41598-020-70610-0>.
70. Nawaz Z, O'Malley BW. 2004. Urban renewal in the nucleus: is protein turnover by proteasomes absolutely required for nuclear receptor-regulated transcription? *Mol Endocrinol* 18:493–499. <https://doi.org/10.1210/me.2003-0388>.
71. Evans SM, Adcox HE, VieBrock L, Green RS, Luce-Fedrow A, Chattopadhyay S, Jiang J, Marconi RT, Paris D, Richards AL, Carlyon JA. 2018. Outer membrane protein A conservation among *Orientia tsutsugamushi* isolates suggests its potential as a protective antigen and diagnostic target. *Tropical Med* 3:63. <https://doi.org/10.3390/tropicalmed3020063>.
72. Izac JR, O'Bier NS, Oliver LD, Jr, Camire AC, Earnhart CG, LeBlanc Rhodes DV, Young BF, Parnham SR, Davies C, Marconi RT. 2020. Development and optimization of OspC chimeritope vaccinogens for Lyme disease. *Vaccine* 38:1915–1924. <https://doi.org/10.1016/j.vaccine.2020.01.027>.
73. Livak KJ, Schmittgen TD. 2001. Analysis of relative gene expression data using real-time quantitative PCR and the 2^{-ΔΔCT} method. *Methods* 25:402–408. <https://doi.org/10.1006/meth.2001.1262>.

74. Faris R, Weber MM. 2019. Identification of host pathways targeted by bacterial effector proteins using yeast toxicity and suppressor screens. *J Vis Exp* <https://doi.org/10.3791/60488>.
75. Sisko JL, Spaeth K, Kumar Y, Valdivia RH. 2006. Multifunctional analysis of *Chlamydia*-specific genes in a yeast expression system. *Mol Microbiol* 60:51–66. <https://doi.org/10.1111/j.1365-2958.2006.05074.x>.
76. Benjamini Y, Drai D, Elmer G, Kafkafi N, Golani I. 2001. Controlling the false discovery rate in behavior genetics research. *Behav Brain Res* 125:279–284. [https://doi.org/10.1016/s0166-4328\(01\)00297-2](https://doi.org/10.1016/s0166-4328(01)00297-2).
77. Yu G, Wang LG, Han Y, He QY. 2012. clusterProfiler: an R package for comparing biological themes among gene clusters. *OMICS* 16:284–287. <https://doi.org/10.1089/omi.2011.0118>.